Towards a Quantum Gas Microscope for Fermionic Atoms

by

VINAY RAMASESH

Submitted to the Department of Physics in partial fulfillment of the Requirements
for the
Degree of

BACHELOR OF SCIENCE

at the

MASSACHUSETTS INSTITUTE OF TECHNOLOGY

May 2012

Signature of Author_____
Department of Physics
May 17, 2012

Certified by_____
Martin Zwierlein
Thesis Supervisor, Department of Physics

Accepted by_____
Professor Nergis Mavalvala
Senior Thesis Coordinator, Department of Physics

To Amma, Appa, and Pati

Towards a Quantum Gas Microscope for Fermionic Atoms

by

Vinay Venkatesh Ramasesh

Submitted to the Department of Physics
on May 17, 2012, in partial fulfillment of the
requirements for the degree of
Bachelor of Science

Abstract

This thesis reports the achievement of a two-species apparatus for use in an upcoming experiment with fermionic ultracold atomic gases. First, we describe the construction of a laser system capable of cooling and trapping gaseous lithium-6 atoms in a 3D Magneto-Optical Trap. Second, we discuss the realization of a 2D Magneto-Optical Trap which, in our experiment, acts as a high-flux source of cold potassium-40 atoms. These two systems are critical first steps in cooling the lithium and potassium atoms to quantum degeneracy.

Thesis Supervisor: Martin W. Zwierlein
Title: Thesis Supervisor, Department of Physics

Acknowledgments

When I first joined the Zwierlein group, I was immediately overjoyed to find myself working alongside so many amazing people. It was apparent from the start that everyone in the group was remarkably talented, but what really floored me was the spirit of camaraderie and excitement that pervaded the group. This spirit made me enjoy myself so much that I decided to stay on for an extra year as a Master's student.

I count myself extremely lucky that I was able to work under Professor Martin Zwierlein for the past two years. The amount of attention Martin is able to give his students is unfathomable. Any time I wanted to ask for help, Martin was more than happy to listen. Quick questions could easily spawn hour-long chats, about anything from lab work and general physics to which classes I should take. I remember one particular day when Martin skipped his lunch to give me advice for an hour about grad school decisions; in fact, this sort of thing happened fairly often. It has been a great pleasure to learn from him, and I hope that my future career will make him proud.

I have also had the good fortune to work under two fantastic post-docs, Peyman Ahmadi and Waseem Bakr. Peyman took me under his wing when I first joined the group. Whenever I found myself overwhelmed by learning all the new lab techniques, I knew Peyman would set me straight in no time. His body of knowledge of atomic physics techniques was amazing, and I relied on it heavily throughout my time here.

Waseem, similarly knowledgeable, struck a great balance between guiding his students and giving us freedom. Perhaps most importantly, Waseem taught me the very valuable lesson that optics tend to mysteriously disappear if left unused for a bit. I'm glad I'll be working with him next year, and hopefully he's finally convinced that the "2D MOT Rumors" are, in fact, not exaggerated.

Thomas Gersdorf was an awesome colleague, mentor, and friend; my time in the lab would not have been nearly as fun without him. He is my model of what I hope to be in grad school; most of all, I hope I have picked up at least some of his relentless drive. Dave Reens was both a terrific co-worker and a great travelling buddy. I

thoroughly enjoyed all of our long discussions and debates, and while I wish both Dave and his fiancée all the best in Colorado, I'm sad to see him leave; together, we would have been unstoppable. Melih Okan, Takuma Inoue, and Jordan Goldstein completed the Fermi II family, and it will be quite hard to leave all of them next year.

The BEC I and Fermi I crews were a large part of what made day-to-day CUA life fun: Ariel Somner, Mark Ku, Lawrence Cheuk, Ibon Santiago, Peter Park, Cheng-Hsun Wu, Sebastian Will, and Tarik Yefsah. Ibon and I worked closely together when I started out in the group, and I am very grateful to count him both a mentor and a friend. To Tarik, I would like to apologize for rigging the movie night votes, but someone had to show you Iron Man and Sherlock Holmes. To the entirety of Fermi I: sorry for stealing your computers so often.

Outside of our group, thanks to Mark Belanger at the Edgerton shop for teaching me to be a good machinist. If any new student in Martin's group is reading this: sign up for the Edgerton shop now! You'll thank me (and Mark) later.

Dr. Nergis Mavalvala has been a wonderful mentor to me ever since I was in her Junior Lab section. It's obvious that she cares deeply about each of her students, which is probably why every physics major I've ever spoken to has shown nothing but the highest admiration for her. More than anything else, I thank her for the confidence she has shown in me.

Professor Terry Orlando has also been a tremendous influence on my undergraduate career, in addition to being one of the nicest people I have encountered here at MIT. Learning solid state physics from him was immensely enjoyable, and his class on applied superconductivity almost convinced me to go into superconducting qubit research for my graduate studies.

Finally, I would like to thank my family, without whom none of this would have been possible. My parents, Ranga and Nalini Ramasesh, and my grandmother, Lakshmi Ramachandran, deserve far more gratitude than I can express here, or in words at all. The care, love, and support they have given me throughout my entire life have had the greatest influence on making me the person I am today. Above all, I hope that I continue to make them proud.

Contents

List of Figures

Chapter 1

Introduction

1.1 Ultracold Atomic Gases

Ultracold atomic gases provide an opportunity to experimentally study strongly interacting quantum systems in a controlled manner. When these gases are cooled down to temperatures T such that their wavefunctions, with a spread given roughly by the deBroglie wavelength

$$\lambda_{dB} = \frac{h}{\sqrt{2\pi m k_b T}} \tag{1.1}$$

start to overlap (here m is the atomic mass), the quantum nature of the individual atoms starts to play a large role in determining the particle dynamics [9]. In addition, the interactions between atoms in the gas can be experimentally controlled by external electromagnetic fields, allowing the for the realization of a variety of system behaviors in the atomic cloud.

The controllability of atomic interactions gives rise to the possibility of accurately simulating, with atoms, a large range of quantum systems. This is simulation in the spirit of Feynman, who in 1982 envisioned a universal quantum simulator [10]. For example, a cloud of fermionic atoms trapped in an optical standing wave mimics the dynamics of interacting electrons subject to the periodic potentials of crystals [11]. The atomic system has several properties that make it nice to use as a simulator. In addition to the precise control we can exert over the interactions of the cloud, the

atomic system is much cleaner than real condensed matter systems, which possess numerous defects and impurities. Perhaps most importantly, the huge ratio between the mass of the ultracold atoms and that of the electrons they simulate implies that the atomic dynamics are much slower than their electronic counterparts, making it possible to observe these dynamics experimentally.

Usually, the properties of the atomic gas after an experimental run are determined through bulk measurements on the gas. The standard technique of absorption imaging, for example, shines resonant light on the cloud, taking a "shadow" image of the atomic density. From these images, which have a resolution of a couple of μm [11], bulk properties such as the temperature and chemical potential of the cloud can be determined.

Recently, high-resolution optical imaging systems have been built, by Professor Markus Greiner's group at Harvard [12] and by Professor Immanuel Bloch's group at Munich [13], that allow single-site detection of atoms in an optical lattice. In contrast to bulk techniques, this high-resolution system enables direct measurements on individual optical lattice sites. This "quantum gas microscope," built on an apparatus which uses a gas of ultracold ^{87}Rb atoms, achieves a resolution of roughly 600 nm, enough to detect the occupany of single lattice sites. With such detection capabilities, images like the one shown in figure 1-2 can be obtained. These images have enabled the direct detection of quantum phases such as the Mott insulator [14]. Further, single-site measurements give rise to the possibility of directly measuring quantities like correlation functions, which previously were unobtainable. Thus far, however, the only quantum gas microscopes in existence have been used for bosonic atoms, such as ^{87}Rb.

1.2 Present experiment

This thesis describes a new experiment being built in Professor Martin Zwierlein's research group at MIT, which will consist of a quantum gas microscope for fermionic atoms. Figure 1-1 shows a cartoon of this system. Our experiment will be a double-

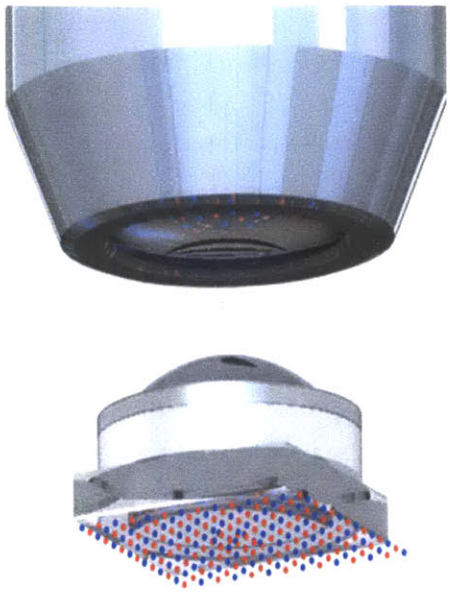

Figure 1-1: Cartoon rendering illustrating the concept of a quantum gas microscope. Created by Thomas Gersdorf.

species experiment using the atoms ^{6}Li and ^{40}K, both fermionic isotopes. Since electrons in solids are fermions, this system, compared to its bosonic counterparts, will more closely resemble the condensed matter systems we are trying to simulate.

As one example of the simulation we hope to accomplish, we note that an important goal of the ultracold atom community at this time is the realization of antiferromagnetism with fermions in optical lattices. This goal, in turn, is a step along the direction of simulating high-temperature superconductivity with ultracold gases [15]. The ability to measure the spin state of atoms on individual lattice sites would, for example, allow direct detection of such antiferromagnetic ordering.

1.3 Outline of this thesis

In the following chapters, I summarize my contributions to the construction of a quantum gas microscope. A preliminary step in achieving quantum gas microscopy of fermions is the construction of an apparatus capable of cooling and trapping these atoms. While the ultimate goal of our efforts was the construction of the microscope,

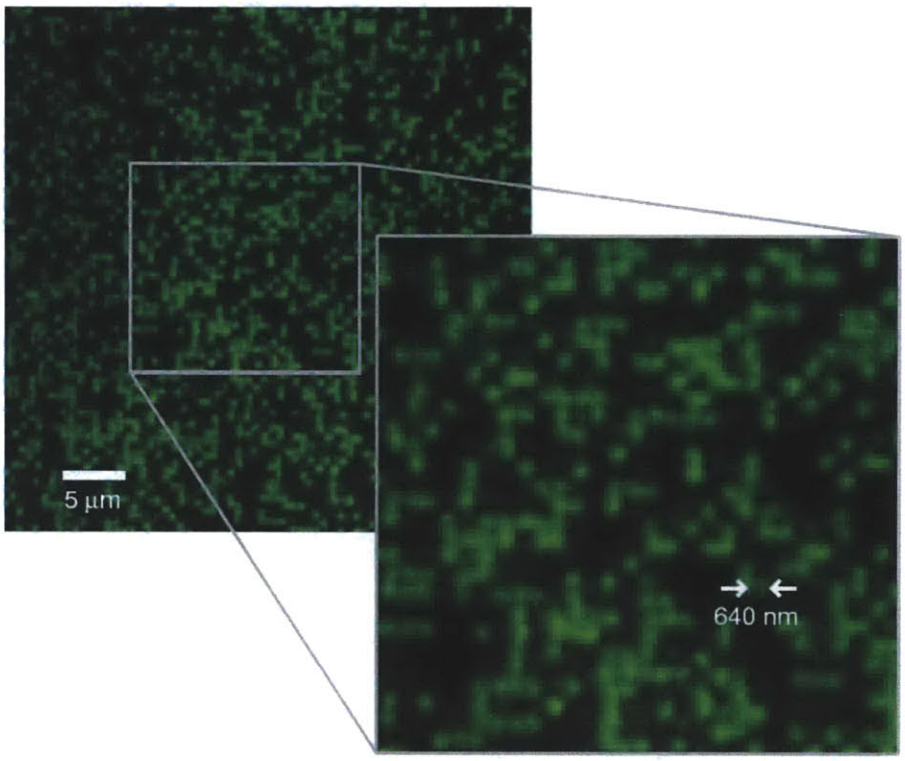

Figure 1-2: An example image obtained with the quantum gas microscope built in Professor Greiner's group at Harvard. Figure obtained from Professor Greiner's website.

the techniques I describe here, namely laser cooling and magneto-optical trapping, are staples of atomic physics experiments in general. My aim is to introduce these techniques to students entering Professor Zwierlein's group with the same background I had when I initially joined, namely, coursework in mechanics, electricity and magnetism, waves, and first-semester quantum and statistical mechanics.[1] Some of the concepts presented here require more advanced quantum mechanics; where appropriate, references have been provided for the interested reader.

The thesis is organized as follows:

Chapter 2 presents the theoretical background necessary for understanding the work. We first present the electronic structures of ^{6}Li and ^{40}K. After discussing the forces resonant laser beams exert on atoms, we treat basic methods of cooling and trapping neutral atoms: optical molasses, and both 2D and 3D magneto-optical traps.

Chapter 3 describes the laser system constructed for cooling and trapping ^{6}Li atoms. We discuss the standard methods of frequency-stabilizing a diode laser to an atomic transition, Doppler free and frequency-modulation spectroscopy. After this, we describe the techniques used to shift the frequencies of the laser beams with acousto-optical modulators, after which the beams are amplified by injection locking into slave lasers. The work described in this chapter was largely conducted during the summer of 2011. Eventually, the light generated by this system will be used to slow and trap ^{6}Li atoms; however, our first efforts at microscopy will be with ^{40}K atoms, so the ^{6}Li laser system described here currently lies unused.

Chapter 4 describes the 2D magneto-optical-trap used to pre-cool ^{40}K atoms before loading them into the 3D trap. The laser system which creates the light used in this trap was set up by visiting graduate student Thomas Gersdorf. As of this thesis writing, trapping of the potassium atoms in the 2D mot has been achieved, but the parameters (laser detuning, laser power, magnetic field gradient, etc.) which determine its performance have not been optimized.

Chapter 5 concludes the thesis, describing work which will be undertaken in the

[1]For those steeped in the MIT lingo, these courses are 8.022, 8.03, 8.033, 8.04, and 8.044, the standard courses a sophomore-level MIT physics major would have completed.

near future to get the microscope up and running.

Chapter 2

Theoretical Background

The main achievement reported in this thesis is the realization of equipment to cool and trap gaseous ^{6}Li and ^{40}K. Laser cooling techniques, the invention of which resulted in the 1997 Nobel Prize (see the Nobel Lectures [16], [17], and [18]), allow us to cool the motion of an atomic gas by exploiting our knowledge of an atom's internal states and their coupling to resonant laser fields. As such, we begin the theory chapter of this thesis with a section summarizing the relevant properties of ^{6}Li and ^{40}K atoms. Section 2 of this chapter explains the forces that near-resonant laser beams exert on atoms, which leads into sections 3 and 4 on Doppler cooling and magneto-optical trapping (MOT), respectively. In section 5, we discuss techniques to load 3D MOTs, specifically the theory behind the 2D MOT which we use for potassium atoms.

2.1 Properties of our Atoms

Lithium and potassium, the atoms we use in this experiment, have both bosonic and fermionic isotopes. Lithium comes in both lithium-7, with a natural abundance of 92.5%, and lithium-6, with an abundance of 7.5% [1]. Lithium-6 is a fermion, while lithium-7 is a boson. In the case of potassium, there are three naturally occurring isotopes: potassium-39, with 93.3% natural abundance, and potassium-41, with 6.7% natural abundance, are bosons, while potassium-40, the least abundant isotope, is a fermion. As our experiment concerns fermions, we use ^{6}Li and ^{40}K, which, inciden-

tally, are the only stable fermionic isotopes of alkali atoms.

Both lithium and potassium are so-called hydrogenic atoms with one valence electron. Lithium, with three electrons, has the ground state electronic structure $1s^2 2s^1$, whereas potassium, with nineteen electrons, exhibits the structure $1s^2 2s^2 2p^6 3s^2 3p^6 4s^1$. The outer electron in each of these atoms is known as the "optically active" electron, as it is the transitions of this electron which give rise to the spectra characteristic of these elements.[1]

In contrast to hydrogen, the S and P states of the optically active electron in multi-electron atoms like lithium and potassium are not degenerate. Rather, in both lithium and potassium, they are split by about 2 eV. The origin of this splitting is due to the "quantum defect," expressing an "effective nuclear charge." Its physical origin lies in the fact that S-orbital wavefunctions have a much larger component at low radii than P-orbital wavefunctions. Stated otherwise, an electron occupying an S-orbital state will, loosely speaking, spend much more time near the nucleus than the corresponding P-orbital electron, and so will have less of the nuclear charge screened by the core electrons [3]. Thus, it will sit at a lower energy. This energy difference gives rise to the spectroscopic D-lines of both potassium (780 nm) and lithium (671 nm).

Apart from the quantum defect, the P orbital has its energy level split further by the coupling between the electron's spin and orbital motion, the so-called fine structure [19]. This coupling, mediated by the magnetic interaction between the electron's spin and angular momentum, splits the P orbital into two levels, denoted $P_{1/2}$ and $P_{3/2}$. The subscript here is the value of J, or total electronic angular momentum, in this state. The S orbital does not have a fine-structure splitting because it contains no orbital angular momentum. The exact physics behind the fine structure splitting does not concern this thesis, but the interested reader can refer to chapter 17 of [20]. All of the laser cooling and trapping we perform involves only the higher-lying energy

[1]Strictly speaking, this is only an approximation, neglecting the Coulomb interactions between the electrons themselves. In a multi-electron atom, the energy eigenstates are many-body states, and different energy states vary not only in the occupation of the most energetic electron, but all of them.

state, the $P_{3/2}$.

The final level splitting, which affects both the S and P states, is known as the hyperfine splitting. It arises from the interaction between the electronic and nuclear magnetic moment, but again, the exact physics need not concern us. Its magnitude is much smaller than that of the fine structure splitting because of the small size of the nuclear magnetic moment. In lithium, the hyperfine splitting is 228 MHz and in potassium, it is 1.77 GHz. The various hyperfine sub-levels are labeled by their value of F, or total electronic and nuclear angular momentum.

Taking into account all of the splittings mentioned above, the energy-level diagrams for the optically active electron in both lithium and potassium are shown in figures 2-1 and 2-2. Laser cooling and trapping requires atoms to continuously absorb and re-emit photons. Thus, of particular interest to us are so-called cycling transitions. These transitions connect particular atomic states such that an atom in the higher of the two states will, due to selection rules, only fall down into one and only one other state, it's "cycling partner." For alkali atoms, the $^2P_{3/2}$ state with the highest value of F and the the $^2S_{1/2}$ states with the highest value of F are cycling partners. These states form an almost ideal two-level system [21].

Unfortunately, when working with the cycling transition of an atom, there exists a finite probability of exciting the atom into the wrong hyperfine state, from which it can fall back into the ground state other than the one it was originally in. To account for this possibility, we include a laser beam at the right frequency to excite atoms from this "dark" ground state back into the right hyperfine level. This transition, called the repumping transition, is also shown on the energy-level diagrams on the next two pages. The repumper is particularly important for lithium, in which the upper hyperfine levels are spaced so closely as to not be spectroscopically resolvable. Because of this close spacing, the probability of exciting an atom into the wrong hyperfine level is larger for lithium than it is for potassium, in which the upper hyperfine levels are clearly resolved.

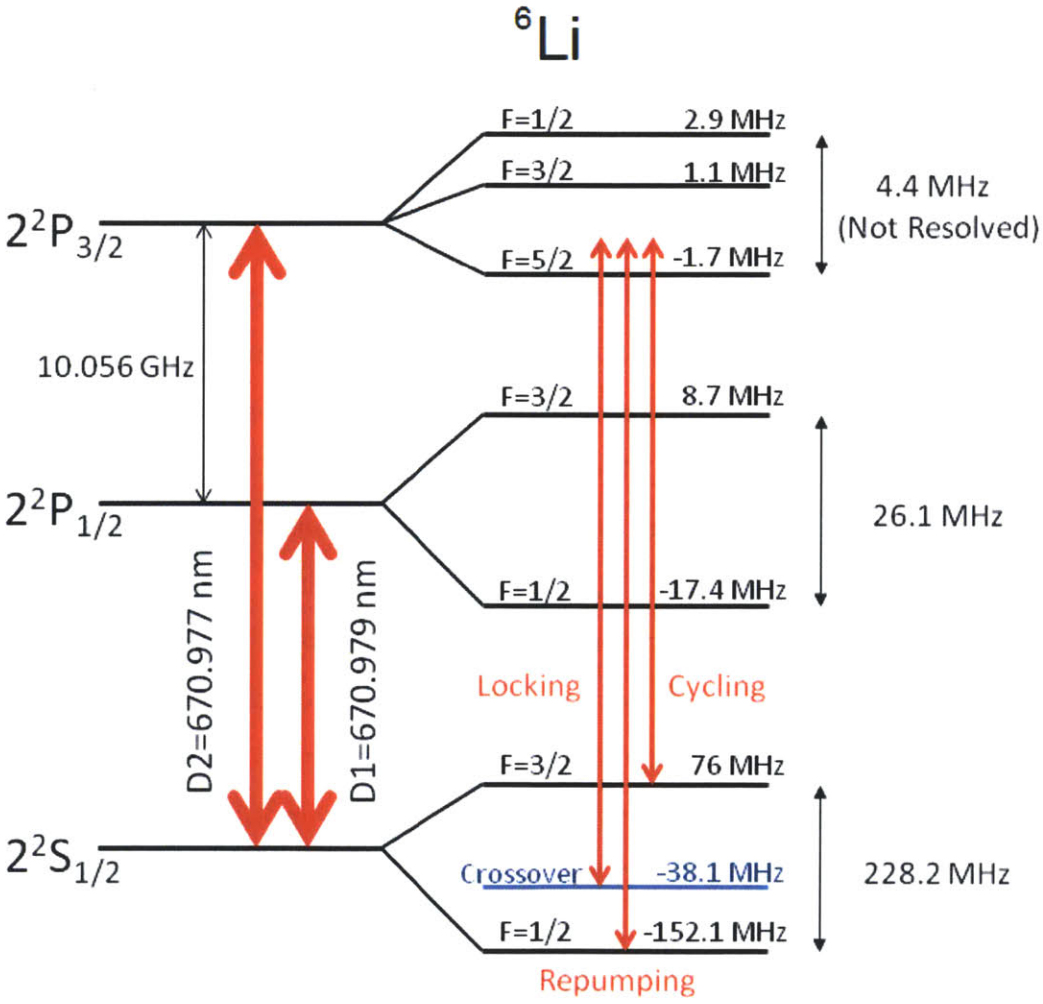

Figure 2-1: Level structure of lithium-6. Figure adapted from [1].

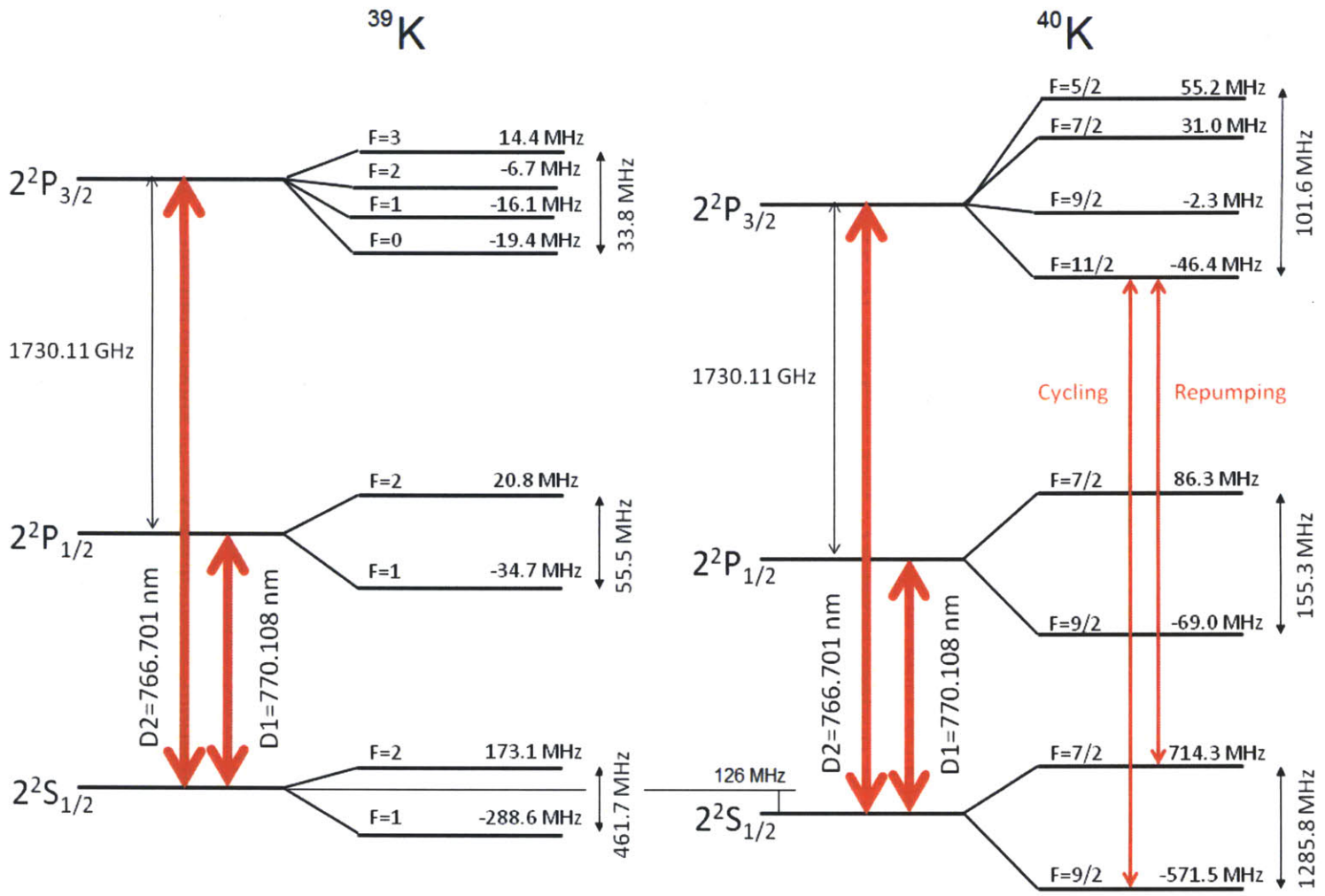

Figure 2-2: Level structure of potassium-39 and potassium-40. Figure adapted from [2].

2.2 Light forces

Laser cooling and trapping involves the use of laser light to exert forces on atoms, thus achieving some degree of control over their motion. The nature of this light force can be derived in a straightforward manner using the language of density matrices and along the way making the rotating wave approximation, which neglects the effects of non-resonant frequency components of the laser field. Such an approach is carried out in detail in [22]. Here, we briefly summarize the results and provide some physical motivation.

Consider a laser beam of wavevector $\mathbf{k}$ and frequency ω_0 shining from a particular direction on an atom or cloud of atoms. Let the energy difference between the two states addreessed by the laser, $|e\rangle$ and $|g\rangle$ be $\hbar\omega$. Given a laser beam with an electric field of the form $E_0 \cos\omega_0 t$, the strength of the coupling between the ground and excited states can be described by the Rabi frequency Ω, where $\hbar\Omega = E_0\langle e|q_e r|g\rangle$. The strength of the laser beam can be described by the dimensionless saturation parameter, $s_0 = 2\Omega^2/\Gamma^2$. The difference between ω and ω_0 is known as the *detuning* of the laser beam, denoted by δ. One last bit of terminology: situations in which the laser frequency is higher than the transition frequency are known as by *blue* detuning, whereas when the laser frequency is lower than the transition frequency, the situation is referred to as *red* detuning. With these terms out of the way, we can proceed to describe the relevant light force formulas.

The momentum carried by each photon in the beam is given by $\hbar\mathbf{k}$. When an atom absorbs such a photon, this momentum is transferred to the atom. For the cycling transitions described earlier, the atom will, after a time roughly given by $1/\Gamma$ (the linewidth of the transition), spontaneously emit another photon and fall back into its cycling partner state. This process of absorption followed by spontaneous emission repeats several times, and the atom receives momentum kicks from both absorption and emission. On average, the momentum kicks due to all of the spontaneously emitted photons sum to zero, as the atom radiates equally into all directions. So the force on the atom arises almost entirely from the absorbed photons, and is equal to

the individual momentum kick $\hbar\mathbf{k}$ times the absorption rate, which in equilibrium is equal to the emission rate. This rate, Γ_s, is the product of the excited state occupany and the decay rate Γ, which is given by

$$\Gamma_s = \frac{\Gamma}{2}\frac{s_0}{1 + s_0 + (2\delta/\Gamma)^2} \tag{2.1}$$

The light force is then equal to

$$\mathbf{F} = \hbar\mathbf{k}\Gamma_s = \hbar\mathbf{k}\frac{\Gamma}{2}\frac{s_0}{1 + s_0 + (2\delta/\Gamma)^2} \tag{2.2}$$

For potassium, the saturation intensity, corresponding to $s_0 = 1$, is 1.77 mW/cm^2. For lithium, it is 2.5 mW/cm^2.

Note the dependence of the above formulas on the detuning parameter δ. As the magnitude of δ increases, the force on the atoms decreases. Qualitatively, this can be understood by the fact that the closer a beam is to an atomic resonance, the more strongly it will be absorbed.

2.3 Doppler Cooling

The dependence of the light force on detuning, combined with the Doppler effect, led to a 1975 proposal by Hänsch and Schawlow to cool atoms with near-resonant laser light [23]. This technique is known as Doppler cooling, or the optical molasses technique.

The key idea behind Doppler cooling is remarkably simple, and we describe it first in one dimension. The set up involves two counterpropagating ("head on") laser beams, red detuned from the atomic cycling transition. In the lab frame, both of these beams have the same frequency, but because of the Doppler effect, a moving atom will see the laser beams at different frequencies: the detuning between the atom and the beam it moves towards decreases, while the detuning between the atom and beam it moves away from increases. This leads to the atom preferentially absorbing photons whose momentum is in the opposite direction to its velocity, thus slowing

the atom down.

To analyze this more quantitatively, note that the frequency at which an atom, moving with velocity v, sees the laser beam goes as $\omega_D = \omega_0 \pm kv$, meaning that the detunings become $\delta_D = \delta \pm kv$. Thus, the light force on the atoms is, referring back to eqn. (2.2), is

$$\mathbf{F} = \mathbf{F}_1 + \mathbf{F}_2 = \hbar \mathbf{k} \frac{\Gamma}{2} \left(\frac{s_0}{1 + s_0 + (2(\delta - kv)/\Gamma)^2} - \frac{s_0}{1 + s_0 + (2(\delta + kv)/\Gamma)^2} \right) \quad (2.3)$$

Taylor-expanding this expression around $v = 0$, we find that the force on the atoms is effectively a damping force proportional to the atoms' velocity:

$$\mathbf{F} = -\frac{8\hbar k^2 s_0 \delta}{\Gamma(1 + s_0 + (2\delta/\Gamma)^2)^2} \times v \quad (2.4)$$

Comparing this Taylor approximation with the full result, we find that its validity only extends to the range of velocities roughly between $-\Gamma/k$ and $+\Gamma/k$. We can think of this velocity as, roughly, the "capture velocity" of the molasses.

The extension of this idea to three dimensions is straightforward: rather than two counterpropagating beams, we simply use six, two for each axis.

2.4 Magneto-Optical Trapping

The Doppler cooling scheme above compresses the velocity spread of the atomic cloud, but does not localize the atoms in real space. That is, atoms in an optical molasses can slowly drift away; they are not confined to any preferred location. To perform experiments on the atoms, we would like them to be trapped in the true sense. The first stage of trapping is known as the magneto-optical trap, or MOT (see [3] for an introduction). As with the molasses, we will first illustrate the idea of the technique in one dimension.

The construction of the MOT is similar to that of optical molasses. We begin with two counterpropagating, red-detuned laser beams, as shown in Figure 2-3. However, in the MOT setup the polarization of the beams becomes important. Both beams

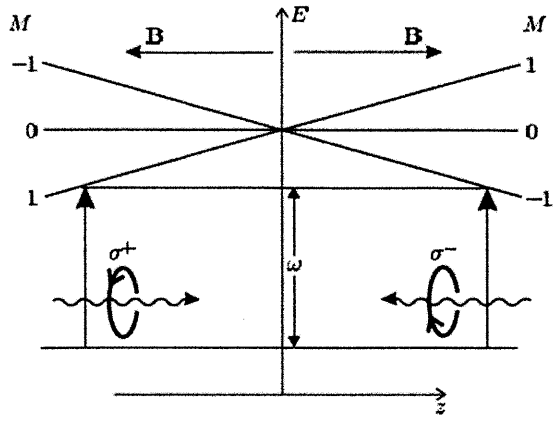

Figure 2-3: The energy level diagram of an atom in an inhomogenous magnetic field used in magneto-optical trapping. Figure taken from [3]

are circularly polarized: the beam moving towards the left has helicity σ_-, while that moving towards the right has helicity σ_+. Now, as the name"magneto-optical trap" suggests, we add a magnetic field $B(z) = bz$. Due to the Zeeman effect, the magnetic field splits the upper energy levels of the atom into three separate levels, labeled the $m = -1, 0$, and $+1$ sublevels. Due to selection rules, σ_- radiation can only excite transitions from the ground state to the $m = -1$ level, while σ_+ radiation can only activate the $m = +1$ level. Looking at the energy-level diagram shown in figure 2-3, we see that when the atom is to the right of the magnetic field zero-crossing, the $m = -1$ transition is much closer to resonance than $m = +1$, so the atom will absorb much more σ_- light than σ_+ and thus get pushed back towards the zero-crossing. The opposite situation exists to the left of the zero-crossing: the atom will preferentially absorb σ_+ light and get pushed towards the right. This creates a position-dependent force which, in combination with the molasses force, tends to localize atoms near the zero-crossing of the magnetic field.

The magnetic fields used in a 3D-MOT are typically produced by a pair of anti-Helmholtz coils, as shown in figure 2-4.

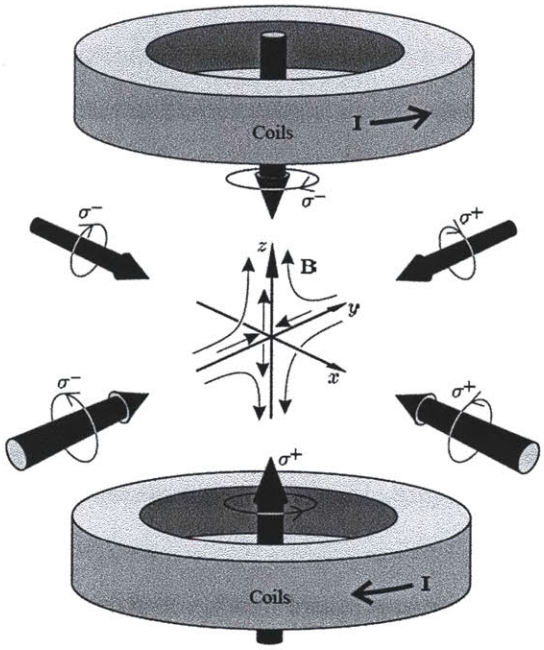

Figure 2-4: Coils producing the 3D-MOT magnetic fields, along with the six laser beams which provide the actual confining force. Figure taken from [3]

2.5 MOT Loading Techniques

The capture velocity of MOTs is similar to that of optical molasses, roughly Γ/k. For both lithium and potassium atoms, this value is on the order of 10 m/s. This means that atoms in a vapor cell at several hundred degrees Kelvin, with velocities of several hundred meters per second, are less than ideal for direct MOT loading. Instead, techniques have been developed to create a slow beam of atoms to load a MOT. The two techniques we use are Zeeman slowing (for lithium) and a 2D MOT (for potassium). The Zeeman slower used in our experiment is documented in a previous undergraduate thesis from our group, see [6]. Here we describe only the 2D MOT technique.

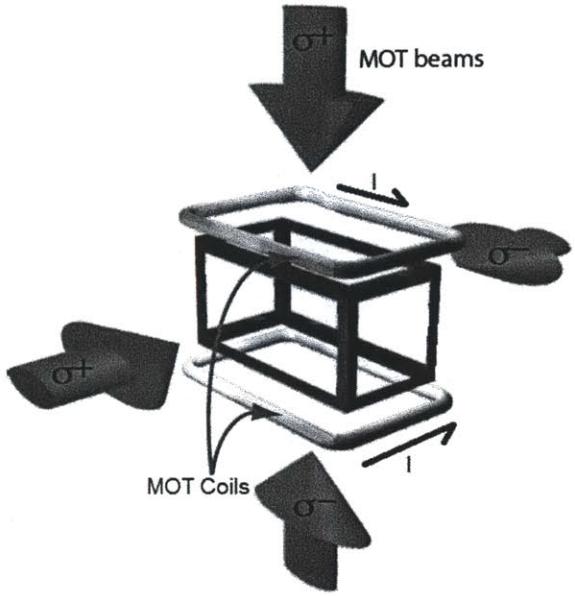

Figure 2-5: 2D MOT setup used by researchers in ETH Zurich. In contrast to a 3D MOT, the confining beams have an elliptical cross-section, creating a cigar shaped atomic cloud. Figure taken from [4]

2.5.1 2D Magneto-Optical Traps

The physics behind a 2D MOT is almost exactly the same as that described in the previous section in reference to 3D MOTs. The main difference between the two is that in a 2D MOT, we only confine the atoms in two directions and allow them to move freely in the third, creating the atomic beam that loads the 3D MOT.

The design of the 2D MOT is shown in figure 2-5. Rather than having six laser beams, a 2D MOT only has four, creating confinement in two dimensions. Not shown in the picture, however, is the aperture connecting the 2D MOT chamber to the chamber which houses the 3D MOT. This aperture, of roughly 2 mm, ensures that only slow-moving atoms make it into the 3D MOT chamber, in the following manner. To successfully get cooled in the 2D MOT and make it through the aperture, the velocity of the atoms along the aperture axis must be small enough that the atoms stay within the trapping region until they are cooled to low radial velocities. If this were not the case, the atoms would escape the trap with enough of a radial velocity component to miss the aperture and thus not make it out of the 2D MOT chamber.

Because of this, the atomic beam coming out of the 2D MOT exhibits a low velocity that is comparable to the capture velocity of a 3D MOT.

With the pure 2D MOT, atoms escape from both ends of the cigar-shaped trap. Only the beam exiting from the end near the aperture, however, will be useful for the 3D MOT. As the other atoms are simply wasted in this case, it would be more desirable to have atoms exit out of only one side of the MOT. To that end, the so-called 2D-MOT-with-push-beam scheme supplements the pure 2D MOT with a fifth laser beam which "pushes" the atomic beam into the 3D MOT chamber. This laser beam both acts as a pushing beam and a plug to prevent atoms from exiting the MOT at the wrong end. The 2D MOT with push beam has been used for ^{40}K by researchers in Zurich to obtain 3D-MOT loading rates of up to $(6.5 \pm 2.0) \times 10^9$ atoms/s, about five times higher than the $(1.2 \pm 0.4) \times 10^9$ atoms/s without a push beam [4].

Another modification to the pure 2D MOT is the so-called 2D$^+$ MOT, which adds not just one, but two transverse laser beams (the "pushing" and "retarding" beams) to the pure MOT, as shown in figure 2-6. This effectively adds an optical molasses in the third direction. However, this optical molasses can be tuned by changing the relative intensities of the pushing and retarding beam. Using this scheme, with a pushing beam six times more intense than the retarding beam, researchers in Paris have obtained 3D MOT loading rates of up to 1.2×10^9 atoms/s.

In our experiment, we use a 2D$^+$ MOT, the construction of which will be described in chapter 4.

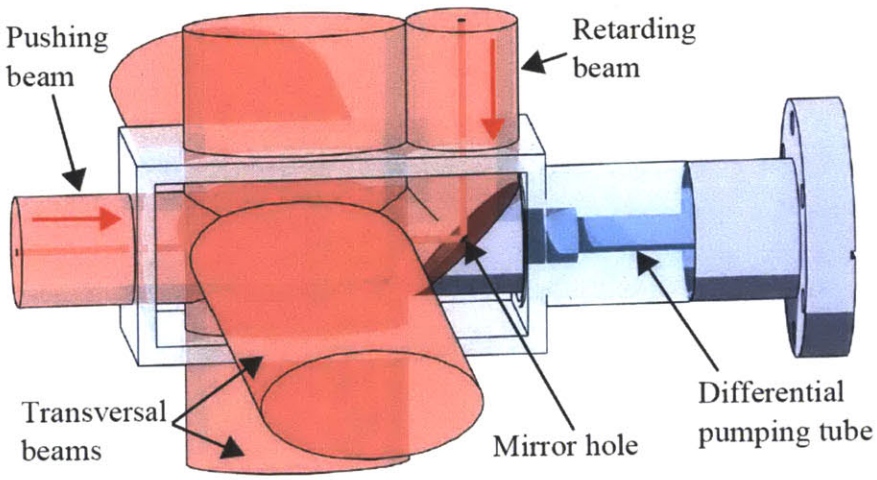

Figure 2-6: Schematic of 2D MOT setup used by researchers in Paris. Figure taken from [5]

Chapter 3

Lithium-6 Laser System

In this chapter we describe the laser system constructed for addressing gaseous ^{6}Li atoms. Specifically, the laser system includes the light which slows the hot lithium atoms (400° C) in the Zeeman slower and then traps them in the first stage of the experiment, the magneto-optical trap (with temperatures on the order of a few milliKelvin). This light does not, however, include that which creates the optical lattice or microscope beams.

Briefly, the laser scheme described here is as follows. Starting with a commercially available laser diode which lases at 671 nm ("the master"), we use frequency-modulation (FM) spectroscopy to lock its frequency at a known offset from the relevant ^{6}Li transitions. The light is then amplified by a commercial Tapered Amplifier and split into separate beams which are frequency-shifted by acousto-optical modulators (AOMs). Once the desired frequencies are obtained, the light is further amplified by a technique known as injection-locking. This amplified light is coupled into optical fibers which carry it from the optical table to the experimental table. This chapter describes each of these steps in greater detail.

3.1 Master Diode Laser

The starting point of our laser system is a master laser which provides a small (~20 mW) power output at a frequency which we control very precisely to be at a known

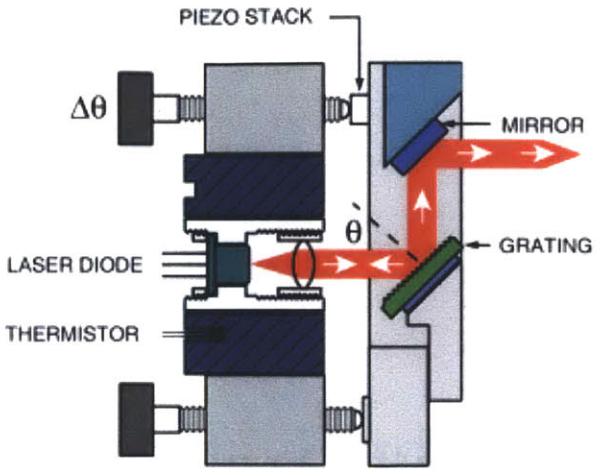

Figure 3-1: The diode laser with added diffraction grating, in the so-called Littrow configuration. Figure taken from [6].

offset from the lithium-6 cooling and repumping transitions. To get an idea of the frequency spread permitted in our master laser, recall that for atomic resonance lines, the absorption spectrum is a Lorentzian curve with an FWHM set by the lifetime of the transition. For our ^{6}Li atoms, this corresponds to an FWHM of about 6 MHz, which means that our frequency lock on the master laser must be at least that good. The technique we use to achieve this degree of frequency stabilization will be described in the next few sections; here, we describe the construction of the master laser itself.

We choose for our master laser a commercially available laser diode from Eagleyard Photonics. In this laser, the gain medium consists of a pn-junction in which electrons "fall down" the bandgap and emit photons [24]. Surrounding the pn-junction are semconductor-air interfaces which act as lossy mirrors, forming the cavity around the gain medium which provides wavelength-selection. The gain profile of the semiconductor medium has a width of about 5 nm or roughly 1000 GHz, centered around 671 nm. Because of the low reflectivity of the air-semiconductor interfaces, the diode laser by itself has a linewidth of about 50 MHz. In view of what we described above, this linewidth is too high for atomic physics experiments.

The linewidth of the diode laser can be substantially reduced by the addition of an external cavity with more reflective mirrors. To add wavelength tunability to our setup, however, we instead add a diffraction grating in front of the diode laser, as

shown in Figure 3-1. This grating is a standard ThorLabs grating with 1800 lines/mm, and allows us to tune the wavelength of the emitted laser beam to the limits of the semiconductor gain profile. The external cavity reduces the frequency spread of the laser to about 100 kHz, suitable for cooling and trapping atoms.

The main factors that influence the wavelength of the laser diode's emitted light are the length of the cavity and the center of the semiconductor gain profile. These factors can be controlled by the temperature of the system, the current injected into the pn-junction, and the angle the diffraction grating makes with the laser diode facet. In our setup, we maintain the temperature precisely to the order of a milliKelvin with a Peltier module. We vary the diode current and grating angle to tune and precisely maintain the output wavelength, as described next.

3.2 Frequency Stabilization Scheme

3.2.1 Doppler-free Spectroscopy

A natural choice for a frequency reference is one of the atomic transitions of ^{6}Li shown in the previous chapter. To perform spectroscopy on individual ^{6}Li atoms as a stepping stone to stabilization, we use a vapor cell of gaseous lithium. Because of lithium's high melting point, the cell must be heated to around 350° C in order to obtain a strong absorption signal.

The cell temperature has an unfortunate consequence for our attempt at spectroscopy: it Doppler broadens each transition line to a signal of unmanageably high spread. To see this quantitatively, note that under Maxwell-Boltzmann statistics, the RMS velocity component of an individual atom in any direction is given by

$$\frac{3}{2} m_{Li} v_{rms}^2 = k_B T \tag{3.1}$$

For T around 350°C, this corresponds to a root-mean-square velocity on the order of 1000 m/s. The Doppler shift associated with this velocity is about a gigahertz for ^{6}Li light of 680nm, which overwhelmingly washes out the 6 MHz natural linewidth we

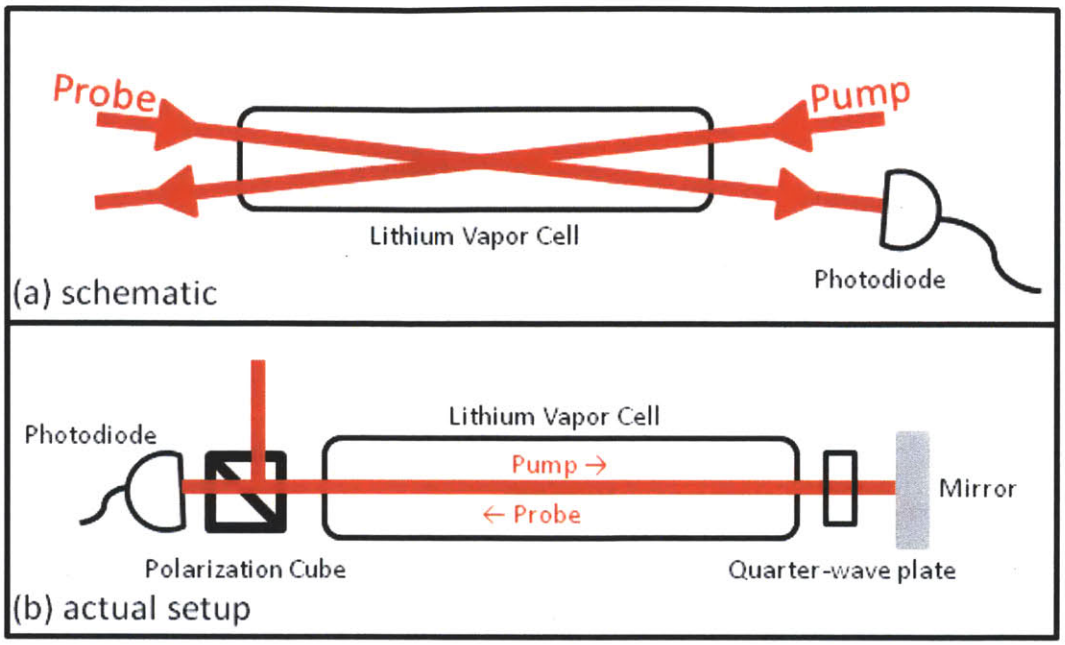

Figure 3-2: Doppler-free spectroscopy setup. (a) schematic view of the setup which is easiest to understand. (b) our implementation of the setup, which uses a retroreflected beam as both the probe and pump beam. A polarization cube allows for the reflection of the pump and transmission of the probe.

would like to see.[1]

Doppler-free spectroscopy, or saturated absorption spectroscopy, is a technique to get around this problem. Its setup is depicted in Figure 3-2. Two counterpropagating beams at the same frequency (called the *probe* and *pump* beams) overlap in the vapor cell and thus interact with the ^{6}Li atoms simultaneously. Only one of the beams, the probe, is detected on a photodiode and gives an absorption signal. As we will show, this technique allows us resolve the hyperfine structure of the atoms.

In the absence of the pump beam, the probe absorption spectrum would look like a Gaussian, Doppler-broadened signal about a gigahertz wide, as we have already described. To see what modifications the pump induces on this background Gaussian spectrum, first note that because the ^{6}Li upper hyperfine levels are not resolvable (their natural linewidth is greater than their spacing), it is safe to regard the ^{6}Li atom as being a Λ-type three-level system with two ground states and one excited

[1]To put things in perspective, this frequency shift corresponds to a wavelength shift of about 0.01nm, still about five orders of magnitude lower than the wavelength itself.

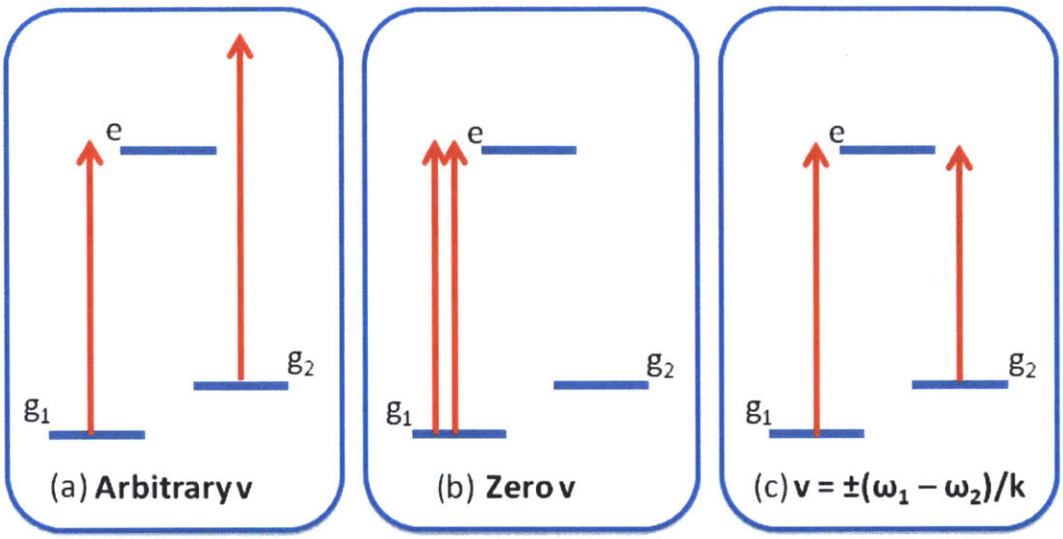

Figure 3-3: Different velocity classes which result in features of the Doppler-free absorption profile. Figure adapted from [7].

state. Let the ground states be $|g_1\rangle$ (with degeneracy 4) and $|g_2\rangle$ (with degeneracy 2), and the excited state $|e\rangle$. Call the transition frequencies between each ground state and the excited state ω_1 and ω_2.

In our setup, the pump and probe beams have the same frequency, say ω, in the lab frame. An atom in the cell moving with velocity v along the direction of the beam will see the pump at frequency $\omega + kv/2$ and the probe at frequency $\omega - kv/2$ (assuming $v \ll c$). Now consider three different velocity classes of atoms in the cell, as shown in Figure 3-3:

For an arbitrary velocity class, shown in fig. 3-3(a), as we sweep the frequency of the pump and probe beam, only one of the beams is resonant with a transition at a given time. This situation yields exactly the same absorption curve as that above, namely a Doppler-broadened profile.

The second velocity class we consider consists of atoms moving with close to zero velocity, shown in fig. 3-3(b). For this velocity class, the pump and probe stay at the same frequency as they are swept, and so when the probe is on resonance with a particular transition, the pump will be too. When this happens, the pump beam causes more atoms than normal to be in the excited state, reducing the number of atoms available in the ground state to absorb probe light. Thus, the absorption of

the probe light is reduced. Note that because this only happens for atoms moving near zero velocity, there is no Doppler shift in this feature, and it shows up on the spectrum with close to its natural linewidth.

The third velocity class actually consists of two velocity classes, namely atoms moving with $v = \pm(\omega_1 - \omega_2)/k$, in fig. 3-3(c). For these atoms, the pump and probe beams are detuned by $\omega_1 - \omega_2$, so when one beam is on resonance with the $|g_1\rangle \rightarrow |e\rangle$ transition, the other beam will be on resonance with the $|g_2\rangle \rightarrow |e\rangle$ transition. Here the pump beam will pump extra atoms into the ground state the probe beam is addressing, resulting in an increased absorption of the probe beam. This feature is known as crossover. Again, because this only happens for a specific velocity class, the width of the crossover trough is determined by the natural linewidths of the two transitions involved, on the order of several megahertz.

So in addition to the background doppler-broadened profile, the absorption signal on the photodiode contains three sharp features: two peaks of reduced absorption corresponding to the zero-velocity atoms, and the crossover trough. Figure 3-4 shows the Doppler-free spectrum for the ^{6}Li-D_2 line, our locking transition. The crossover dip is midway between the two peaks. As seen from the figure, the features have different strengths, determined by the degeneracy of the ground state levels. Because the crossover dip results from contributions from two velocity classes instead of one, it is the strongest feature. We choose to lock our laser to this crossover dip, as its strength gives rise to the possibility of obtaining a more narrow lock than with either of the zero-velocity peaks.

3.2.2 FM Spectroscopy

Upon performing Doppler-free spectroscopy on a vapor cell of ^{6}Li atoms, we have at our disposal a curve of absorption vs. frequency for the given atomic vapor, shown in Figure 3-4. To actually lock our laser to the crossover dip, however, we need an appropriate error signal. The curve itself (fig. 3-4) cannot be used, as it is symmetric about the desired frequency. That is, given an absorption value, our control system will be uncertain whether the current laser frequency is too high or too low. To lock

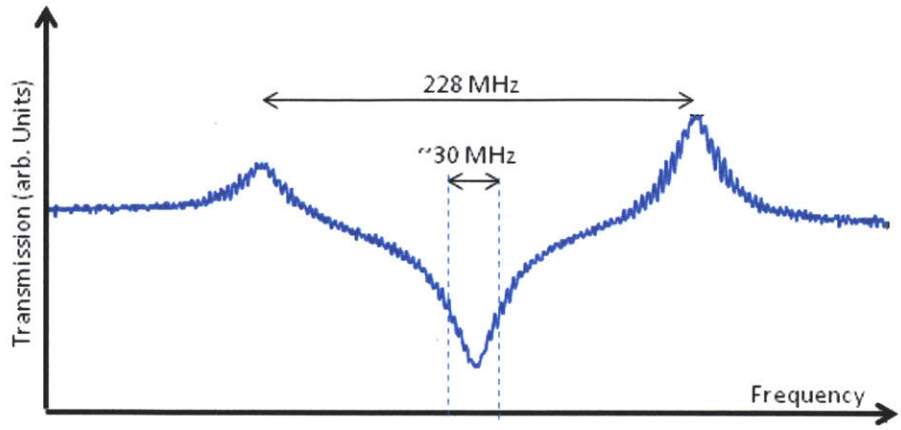

Figure 3-4: The transmission spectrum obtained with the Doppler-free setup. Sizes of features can be estimated by noting that the space between the zero-velocity peaks is equal to the spacing between the two ground hyperfine states of ^{6}Li, 228 MHz. This puts the width of the crossover dip at about 30 MHz, which is larger than the expected 6 MHz due to mechanisms such as collision broadening.

properly, we need an *antisymmetric* error signal.

One solution is to simply differentiate the absorption-frequency curve, yielding a correctly antisymmetric graph. While this solution has been used before with good results (see, for example, [7]), the current widely-used technique is a method known as FM spectroscopy. This method, described in detail by Bjorklund [8], relies on a simple fact: when we are near an atomic resonance, the absorption curve will be symmetric, but the *dispersion* curve will be antisymmetric! This fact can be easily derived from the Lorentz electron-on-a-spring model of atoms; it is nothing more than the fact that as a classical system crosses over resonance, the phase of the oscillations swings from 0 to π in a roughly linear manner at the resonance point.

With the above in mind, we choose to extract the dispersion-frequency curve and use that as an error signal with which to lock. But how to extract the dispersion? The mathematical details are presented in all their glory in [8]. Here, we'll present a more intuitive picture.

Consider first this seemingly unrelated situation: we add two complex exponentials at slightly different frequencies and a phase offset:

$$S = Ae^{i\omega t} + Be^{i(\omega+\Delta\omega t)}e^{i\phi} \tag{3.2}$$

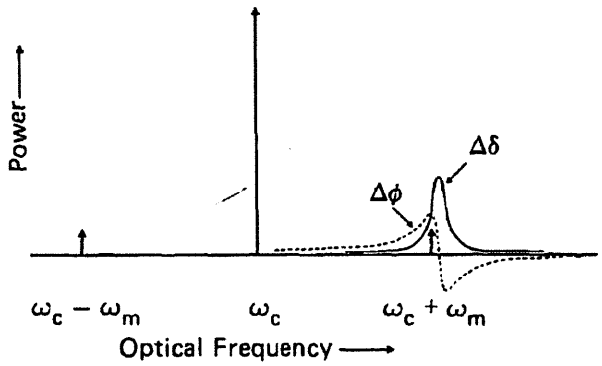

Figure 3-5: The relative scales of the FM modulation frequency and the atomic dispersion and absorption features. Because the modulation frequency is much larger than the scale of these features, only one sideband at a given time (here, the upper sideband) probes the feature. Figure taken from [8].

Let us see what sort of beat signals result. Taking the squared magnitude of the above expression, we get that

$$|S^2| \propto \cos\phi\cos(\Delta\omega t) + \sin\phi\sin(\Delta\omega t) \tag{3.3}$$

If $|\phi| \ll 1$, the above expression reduces (to first order in ϕ) to

$$|S^2| \propto \cos(\Delta\omega t) + \phi\sin(\Delta\omega t) \tag{3.4}$$

So we have something quite simple: the beat signal consists of two components out of phase with each other by 90 degrees: one whose magnitude does not depend to first-order on the phase offset, and one whose magnitude is linearly proportional to this offset.

FM Spectroscopy takes advantage of this ϕ amplitude dependence to measure the dispersion-frequency curve. Starting with the laser beam at frequency ω_c (fig. 3-6(a)), we pass it through an electro-optical modulator (EOM), which adds small ($\sim$ 1%) sidebands at frequencies $\omega_c + \omega_m$ and $\omega_c - \omega_m$(fig. 3-6(b)). With the EOMs used in the ^{6}Li laser system, ω_m was about 50 MHz. We then pass the beam with sidebands through the vapor cell in the same Doppler-free setup as before. Note that because

ω_m is much larger than the natural linewidth of the atomic transition we are probing, only one sideband (say, the upper sideband) will interact with the features of interest at a given time (see fig. 3-5).

Upon leaving the vapor cell, the beam still has three frequency components, but now the one which probed the absorption/dispersion features has been attenuated (by an amount $\exp(-\delta)$) and phase-shifted by the atoms in the cell (by an amount ϕ, i.e. the electric field is multiplied by $\exp(i\phi)$) (fig. 3-6(c)).[2] When we observe this beam on a photodiode, we will see beating due to the three different frequency components. Part of the beat signal will arise from beating between the main ω_c component and the sidebands, and part will arise from beating between the $+\omega_c$ and $-\omega_c$ components. The latter will be negligible compared to the former because the sidebands contain much less power than the main beam. The beating between the ω_c and $\omega_c - \omega_m$ components will be detectable but independent of ω_c. For our purposes, then, the only interesting portion of the photodiode signal is the beating between the upper sideband and the original beam.

The beating between the above two components exactly mirrors the situation considered on the previous page. Applying our results from that situation to this one, we see that the beat sgnal will be two oscillations 90 degrees out of phase. One will have an amplitude proportional to $\Delta\delta$, while the other (the one we want) will have an amplitude proportional to $\Delta\phi$:

$$I \propto \Delta\delta \cos\omega_m t + \Delta\phi \sin\omega_m t \tag{3.5}$$

Mixing this signal with a sinusoid at ω_m—the phase of which we can control—allows us to select out either the $\Delta\delta$ (dispersive) component, which we can use for an error signal. In practice, this phase adjustment is done either by varying ω_m very slightly until the right phase is achieved, or by inserting additional cables (i.e. increasing the delay delay) between the photodiode and mixer.

[2]In reality, all the components will have been attenuated and phase shifted by some "background" values, due to reflections from the cell windows, the air in the cell, and other atoms, but we assume that these background shifts are frequency independent and thus can be neglected.

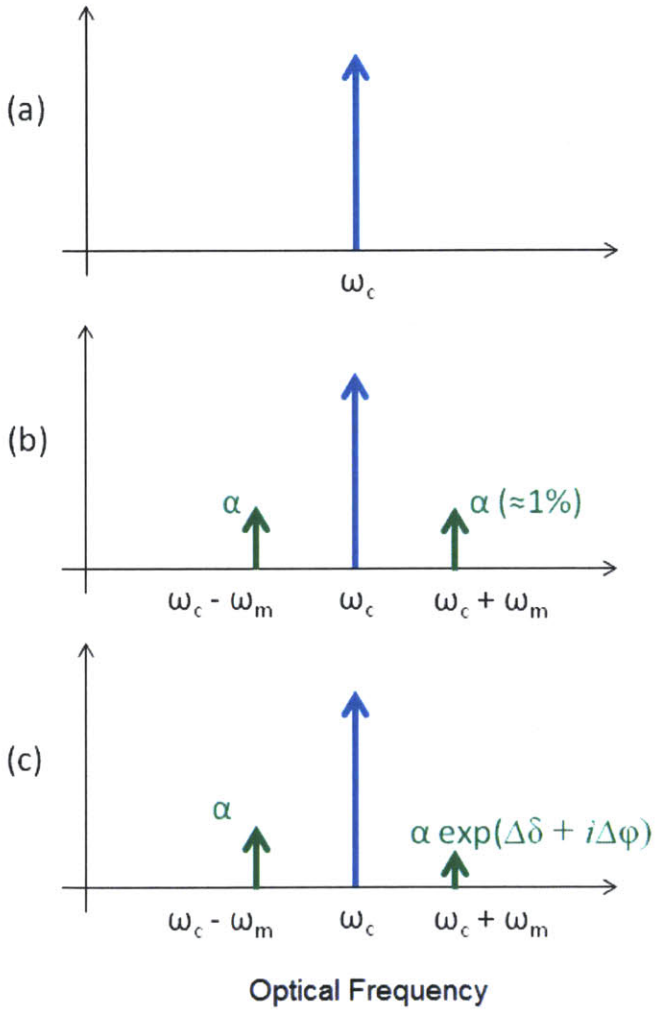

Figure 3-6: Spectrum of the laser beam at various points in the FM spectroscopy pathway. (a) original laser beam, (b) beam after passing through an EOM, and (c) beam after passing through the vapor cell in a Doppler-free setup. This figure corresponds to the situation in which only the upper sideband of the beam sees non-zero absorption and dispersion from the atoms.

The end result of this process is the sought-after antisymmetric error signal: the dispersion curve. Before continuing to describe how we use this error signal to lock the laser, we take a short detour to discuss the workings of an EOM and EOM driver box.

Electro-Optic Modulators

As stated in the previous section, the function of an electro-optic modulator is to add sidebands to a laser beam. The EOM itself is a crystal which exhibits the Pockels effect, meaning its index of refraction changes in response to an applied electric field [25]. We place the crystal between two electrodes (forming a capacitor) wired up to an inductor such that the resonant frequency of this LC-circuit is near our desired ω_m. Into this circuit we couple RF power at ω_m from an EOM driver box (described in the next section). This causes the EOM's refractive index to oscillate in time, following the form $n = n_0 + n_1 \sin \omega_m t$. So when we pass a laser beam with electric field

$$E_{IN} = E_0 e^{i\omega_c t} \tag{3.6}$$

through the crystal, it gets phase-modulated to become

$$E_{OUT} = E_0 e^{i(\omega_c t + kn_0 L + kn_1 L \sin \omega_m t)} \tag{3.7}$$

Assuming $kn_1 L$ is small, we Taylor expand, $e^x \approx 1 + x$, (and throw away the constant $kn_0 L$ phase shift) to get

$$E = E_0 (e^{i\omega_c t} + \frac{kn_1 L}{2} e^{i(\omega_c + \omega_m)t} + \frac{kn_1 L}{2} e^{i(\omega_c - \omega_m)t}) \tag{3.8}$$

Thus, modulating the index of refraction sinusoidally has added sidebands at the modulation frequency.

EOM Drivers

In theory, an EOM driver only needs to output a given amount of RF power at the modulation frequency we want to use. While we could design a dedicated driver to solely perform this task, we instead integrate it with the mixer described earlier. The schematic of our homebuilt EOM driver is shown in Figure 3-7. A voltage controlled oscillator generates an initial RF signal with an amplitude of about +10 dBm. This signal is split, with one portion feeding a voltage-variable attenuator that allows us to control the final output power. From the attenuator the signal passes through a 2W amplifier to give the final output signal used to drive the EOM. The other portion of the VCO output signal feeds one of the input ports of the mixer. The other mixer input is a heavily amplified (40 dB) photodiode signal. As discussed before, the output of the mixer is the error signal we use to lock the master diode.

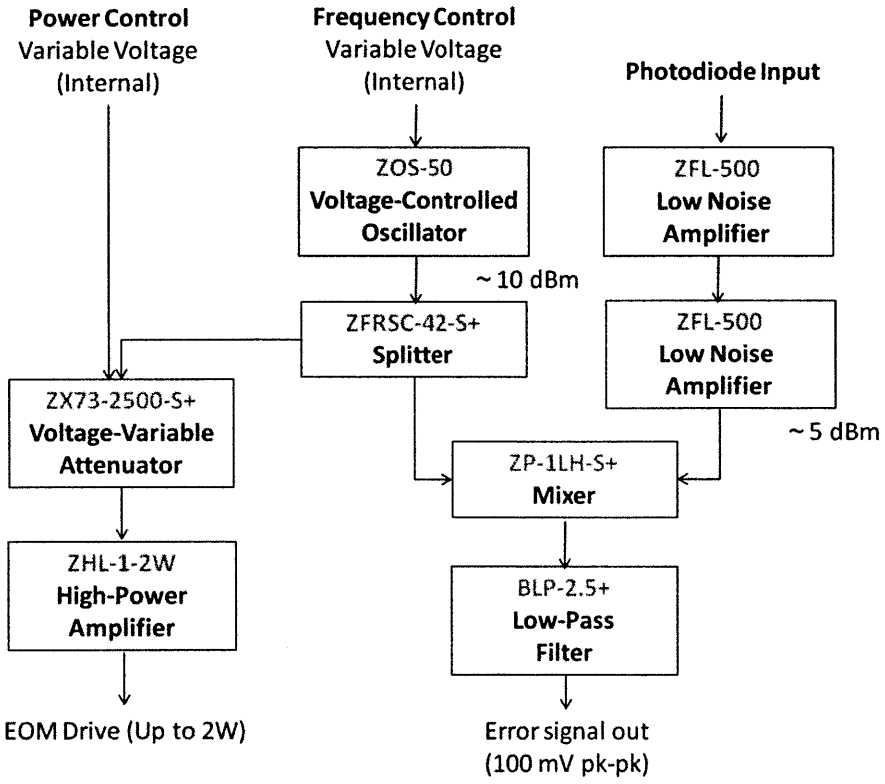

Figure 3-7: EOM Driver Schematic, with Mini-circuits parts numbers. .

One aspect of our EOM driver box that can easily be improved concerns the

placement of the 2 Watt amplifier. The current design houses the amplifier in the same chassis as all of the other components, including the mixer which receives the photodiode signal. Placing the amplifier in its own housing would likely decrease the amount of noise picked up by the other RF components, as the amplifier radiates quite a bit of RF noise. Since this radiation is at the same frequency as the photodiode signal, it can reduce the signal-to-noise ratio of the eventual error signal we want to lock to. A separate housing for the amplifier will likely improve the quality of the error signal, and thus the lock.

3.2.3 Locking the Laser

Given an error signal, the problem of locking the laser to a desired point is a standard problem in the theory of feedback systems. Accordingly, we employ a standard feedback controller suited to our needs, the so-called proportional+integral, or P+I controller. This type of controller uses both the error signal itself and its time-integral as a control signal. A P+I controller is nice because it eliminates the steady-state error or "proportional droop" that often occurs when using just the error signal itself as a control. For an accessible introduction to these ideas, see [26].

In our case, we make a slight modification to the standard P+I compensator: the proportional signal controls the current fed to the laser diode, while the integral controls the grating angle. The reason for this is simple: the grating PZT simply cannot respond fast enough (it is limited to roughly kHz response speeds) to track the proportional error signal. By contrast, an integrator is a natural low-pass filter and is thus perfectly suited to control the grating PZT.

The block diagram of our system is shown in Figure 3-8. The circuit to implement it was designed by Sara Campbell and Cheng-Hsun Wu and is thoroughly described in [6].

At this point, it is perhaps worthwhile to discuss the reasons for choosing an FM-spectroscopy syle locking scheme rather than the direct differentiation of the absorption signal as described in [7]. In the direct-differentiation method, the frequency of the laser is modulated with a frequency of about 10 kHz, and the Fourier component

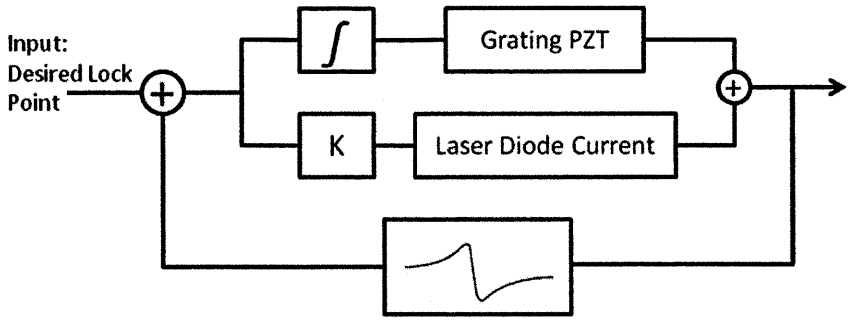

Figure 3-8: Feedback loop corresponding to the P+I controller used in our setup. As shown, the integral of the error signal is used as a control for the grating angle, whereas the proportional signal controlls the laser diode current.

of the absorption signal at 10 kHz is extracted, as it represents the derivative. There are two major drawbacks to this scheme. First, because 10 kHz is much lower than 50 MHz (the EOM modulation frequency), there is far more electromagnetic noise at that frequency floating around in the lab. By contrast, with the 50 MHz modulation, the only noise component at this frequency is the one we introduce ourselves (say, by the amplifier radiating into space and getting picked up by the photodiode signal). This component can be reduced by shielding the amplifier, as is done in our setup. The second drawback to the differentation scheme is that the error signal it yields requires measuring the amplitude of a 10 kHz oscillating signal. As such, the speed of the feedback response is limited to about 10 kHz. With the EOM driver scheme, our feedback system can in principlerespond at up 50 MHz speeds, about 5,000 times faster. This results in a much narrower lock. Of course, there are limits set by the finite response time of the laser diode frequency to current changes and, most importantly, limits in our feedback electronics that typically limit the feedback bandwidtch to about a MHz.

3.3 Acousto-Optic Modulators

As we pointed out earlier, our completed laser system needs to address two different transitions of ^{6}Li, with different detunings for the MOT and slower light. In light of

the frequencies of the ^{6}Li cooling and repumping transition, this requires the output beams to vary in frequency on the order of several hundred megahertz. Shifting the frequency of a laser beam by this amount is a staple of atomic physics experiments and is accomplished with devices known as acousto-optical modulators, or AOMs. In our setup, the AOMs themselves use are commercial, but their driving electronics are homebuilt. Our homebuilt AOM drivers (used for both the ^{6}Li and ^{40}K laser systems) are described in the following section. Here, we describe the workings of AOMs themselves.

In essence, an AOM is a transparent crystal (Tellurium Dioxide, TeO_2, for our wavelength range) in which we use a piezoelectric transducer (PZT) to excite sound waves traveling perpendicular to the laser beam. The interaction between the sound waves and incoming photons causes the desired frequency shift (along with changing both the direction and intensity of the beam).

The standard presentation of an AOMs workings (see, for example, [6] and [7]) describes them in terms of energy and crystal momentum exchange between photons and phonons in the TeO_2. This picture is not the one that the author finds most intuitive, however, so this section will present an alternate derivation that is easier to understand. This formulation has the advantage that anyone with a basic knowledge of diffraction can understand it; knowledge of phonons and crystal momentum is unnecessary.

Consider the excitation of sound waves with a frequency ω_s into the crystal. These sound waves create a periodic variation of the crystals refractive index, of a form

$$n(x) = n_0 + \Delta n \sin(\omega_s(t - \frac{x}{v_s})) \tag{3.9}$$

$$= n_0 + \frac{\Delta n}{2}(e^{i(\omega_s(t-\frac{x}{v_s}))} + e^{-i(\omega_s(t-\frac{x}{v_s}))}) \tag{3.10}$$

$$= n_0 + \frac{\Delta n}{2}e^{i\omega_s t}e^{-i\frac{\omega_s}{v_s}x} + \frac{\Delta n}{2}e^{-i\omega_s t}e^{i\frac{\omega_s}{v_s}x} \tag{3.11}$$

where n_0 is the crystal index of refraction under normal compression, Δn represents the strength of our modulation, v_s is the speed of sound in the crystal, and x represents

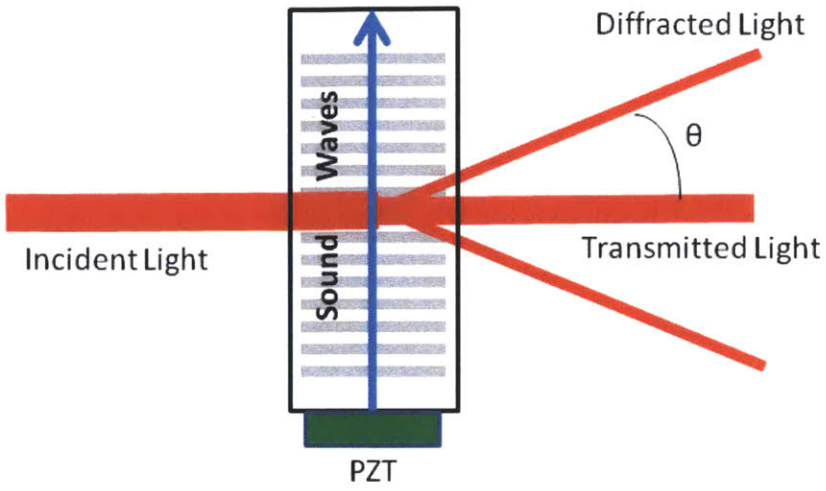

Figure 3-9: Acousto-Optic Modulators. The transmitted light passes through without any change in frequency. The diffracted beams are upshifted and downshipfted by the frequency of the sound waves, and are called the minus- and plus-first order beams, respectively.

the coordinate along the longitudinal crystal direction, perpendicular to the incoming beam.

From basic diffraction theory [27], the far-field diffraction pattern in is simply the Fourier transform of the scattering intensity, which we take to be proportional to $n(x)$. Here the Fourier transform is in terms of the variable $k \sin\theta$, where θ is the angle of the diffracted beam. So, from our expression for $n(x)$ above, we see that the diffracted beam has three components: one which passes through unscathed (the n_0 term), and two scattered beams at angles such that $k \sin\theta = \pm\omega_s/v_s$. The unscattered beam remains at the same frequency; however, because of the exponentials in time, the scattered beams are frequency-shifted, one (the "plus first-order beam") by $+\omega_s$ and the other (the "minus first-order beam") by $-\omega_s$. Ths situation is depicted in Figure 3-9.

Essentially what we have done here is to replace the AOM crystal by moving diffraction gratings, which cause light to be scattered into a plus first and minus first order (the sinusoidal nature of the grating causes all higher orders to be non-existent). The movement of the gratings induces a time-varying phase shift on the scattered beams, which is the same as saying that they are frequency-shifted.

To drive the AOM we couple in RF power to the accompanying PZT. The frequency of this RF signal obviously determines ω_s, while the power controls the intensity of the diffracted beams. Up to a certain point the diffraction efficiency increases with RF power, but after this point a roll-off occurs. For our crystals, the roll-off point is at 1.5-2W of incoupled RF power.

3.3.1 AOM Drivers

The schematic of the AOM drivers built for the lithium and potassium laser systems is shown in Fig. 3-10. As AOM drivers are perhaps the simplest of the various RF electronics used in atomic physics experiments, the schematic is correspondingly straightforward. In view of the previous discussion, the AOM driver must be able to output a controllable amount of RF power at a given frequency. Additionally, we would like to be able to switch the output on and off independently of the driver itself.

Each one of the above requirements leads directly to a single component of the completed driver. All of the RF components are commercial devices purchased from Mini-Circuits^{TM}. The initial RF signal is created by a voltage-controlled oscillator which receives a control voltage either from a potentiometer on the box itself or from an external computer. The (roughly +10 dBm) VCO output passes through a voltage-variable attenuator, which provides anywhere between 3 and 40 dB attenuation of the signal. Varying the control voltage applied to the attenuator allows us to control the output power of the final RF drive signal. Continuing along the signal chain, we meet a TTL-controlled switch, which, like the attenuator and VCO, can be controlled either internally or by an external signal. Finally, the output from the switch is amplified by 29 dB, up to a maximum power of 2 Watts (+33 dBm).

The box is powered by two separate power supplies. One, a 24V linear single-output supply (the Sola Hevi-Duty 83-24-225-3), is reserved solely for the final amplifier. All of the other components (VCO, attenuator, switch) are powered by a Sola SCL 10T515-DN supply. This supply is well suited to the AOM driver because it provides a -15V output in addition to the standard +5V and +15V. The -15V output

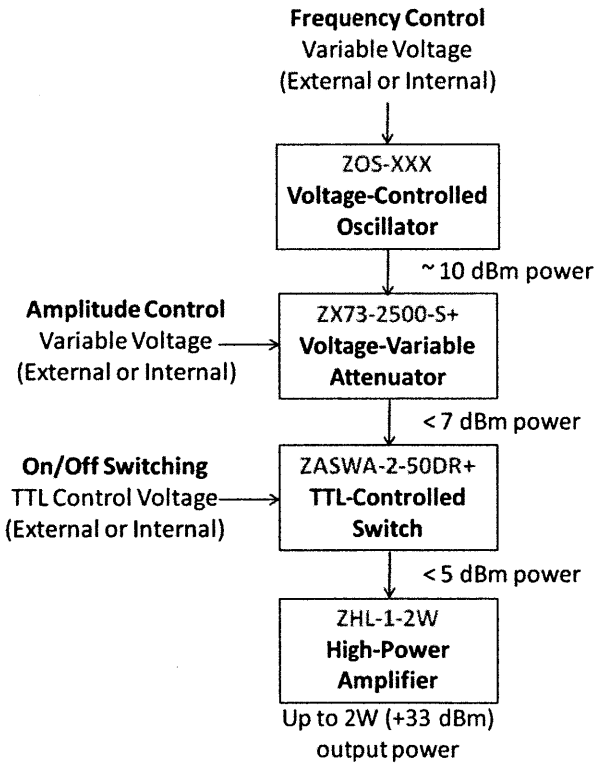

Figure 3-10: Schematic of the AOM Drivers built for the lithium-6 laser system. The ZOS-XXX part is chosen based on the desired frequency of the AOM.

allows us to easily satisfy the TTL switch requirement of a bipolar +/- 5V supply. Other versions of this box have provided a -5V supply for the switch by using an inverting DC-DC converter within the box itself. These boxes have all suffered from a ripple at the switch output due to the nature of the DC-DC converter. With the negative output of the SCL power supply, we can circumvent these problems. Unfortunately, at the time of this writing, Sola no longer manufactures this particular supply.

A couple of features of our particular AOM implementation bear mentioning. First, previous RF electronics built in our group either disregarded or were unaware of torque guidelines for standard SMA connectors. Frequently the connections in these boxes were far over-tightened, leading to RF power leakage. For the currently built drivers, however, we were careful to use the recommended torque of 0.5 Nm on all connections. We observed improvements in power on the order of 1 dB with this proper tightening. Second, to avoid users accidentally powering the 2W amplifier without any load connected (which can easily kill the amplifier [28]), we included power terminators on the front of the box.

In previous experiments in our group, electronics for multiple AOM drivers were housed within a single chassis (see, for example, section 3.5 of [6]). For the current experiment, however, we chose to house each AOM driver in an individual enclosure. This was done for a couple of reasons. First, as each driver includes an amplifier, placing four together in one chassis makes it difficult to properly cool the box and prevent components from overheating. With the individually-housed design, on the other hand, each amplifier can be cooled by its own, dedicated fan. Second, having only components for one driver in a given chassis allows for a much cleaner and more spacious box interior. This makes it easier to perform repairs and adjustments to the box in the future. Lastly, during the early stages of setting up an experiment the drivers are constantly being shuffled around into new uses. With a single box full of many drivers, moving it constantly can be a hassle; with many smaller boxes, it is no problem.

3.4 Amplification

In addition to shifting the frequency of laser beams by passing them through AOMs, we must also amplify their power, as the 20 mW beam which the master diode produces is not nearly enough to cool and trap enough atoms. We amplify the beams in two ways: first, via a commercial device known as a tapered amplifier; and second, by a technique known as injection locking.

3.4.1 Injection Locking

In injection locking, a small amount of laser power (~1-2 mW) is coupled, via an optical isolator, into another laser diode (the "slave") which—at least in the case of the lithium diodes—on its own produces about 100 mW of power.[3] The injected power "pulls" the frequency of the slave to match that of the injected beam, the "master." The slave still produces about 100 mW of power, but now all of this power is concentrated at the master frequency.

The detailed procedure used to injection lock a slave laser is described in [7]. One aspect of this procedure, however, which is not mentioned in that reference is that the particular slave diodes we used only followed the master only at discrete values of slave laser current, roughly about 10 mA apart (although the spacings grew farther apart with increasing current). Because of this, we first scanned the slave current until peaks in the output spectrum were found, and then adjusted the optical components to maximize the peak heights.

3.5 Completed Laser System

With the tools for frequency stabilization, frequency shifting, and amplification described in the previous sections of this chapter, we are now in a position to describe the layout of the constructed ^{6}Li system. A schematic view of the system is shown

[3]For the diodes we use in the potassium laser system, this is not true. The potassium diodes are have anti-reflection coated facets, so they do not have their own cavity and cannot lase on their own at all. Only with seeding do we get a good power output from these diodes.

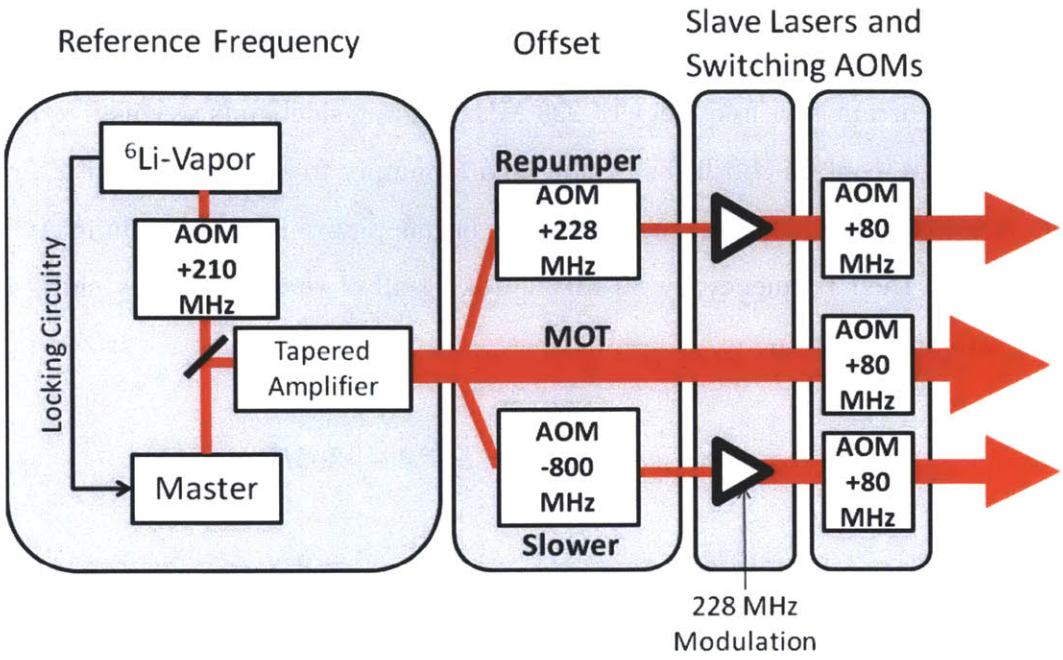

Figure 3-11: Schematic of the completed lithium-6 laser system.

in Figure 3-11.

Looking at the system piece by piece, we start with the "Reference Frequency" section that includes the master laser diode locked to an atomic transition line. As described in a previous section, the reference frequency provided by the ^{6}Li vapor cell is that of the D2 line crossover. In our implementation, however, we do not lock the master laser itself to this feature, but instead we shift the frequency of the laser up by 210 MHz before performing locking. This means that the frequency of the master laser, ν_{mast}, is related to the D2 crossover frequency by

$$\nu_{mast} = D_2^{cross} - 210MHz \tag{3.12}$$

A beam of this frequency feeds a commercial Tapered Amplifier, which amplifies the light from about 18 mW power to close to 350 mW. After exiting the tapered amplifier, the light is split into three different beams. The beam shown on top is the repumper beam, which passes through an AOM that shifts its frequency up by 228 MHz and is then amplified by a slave laser. The middle beam, the MOT cycling beam, proceeds through the slave laser stage with its frequency left untouched. The

last beam, the one for the Zeeman slower, gets passed through AOMs which shift its frequency down by 800 MHz and is then amplified. In this slave laser, however, we modulate the current at a frequency of 228 MHz, adding sidebands at this frequency. This beam, thus, contains both the cycling and repumper frequencies for the Zeeman slower. After the amplification stage, all three beams pass through switching AOMs, which increase their frequency by 80 MHz. Taking all of these frequency shifts into account, we finally obtain

$$\nu_{MOT} = \nu_{mast} + 80MHz = D_2^{cross} - 130MHz \tag{3.13}$$

and

$$\nu_{RP} = \nu_{mast} + 228MHz + 80MHz = D_2^{cross} + 98MHz \tag{3.14}$$

As desired, the MOT and MOT repumper beams are detuned by 228 MHz; this is also the case for the slower, with an additional 800 MHz red detuning from the MOT beams.

Figure 3-12 shows our actual implementation of this laser system.

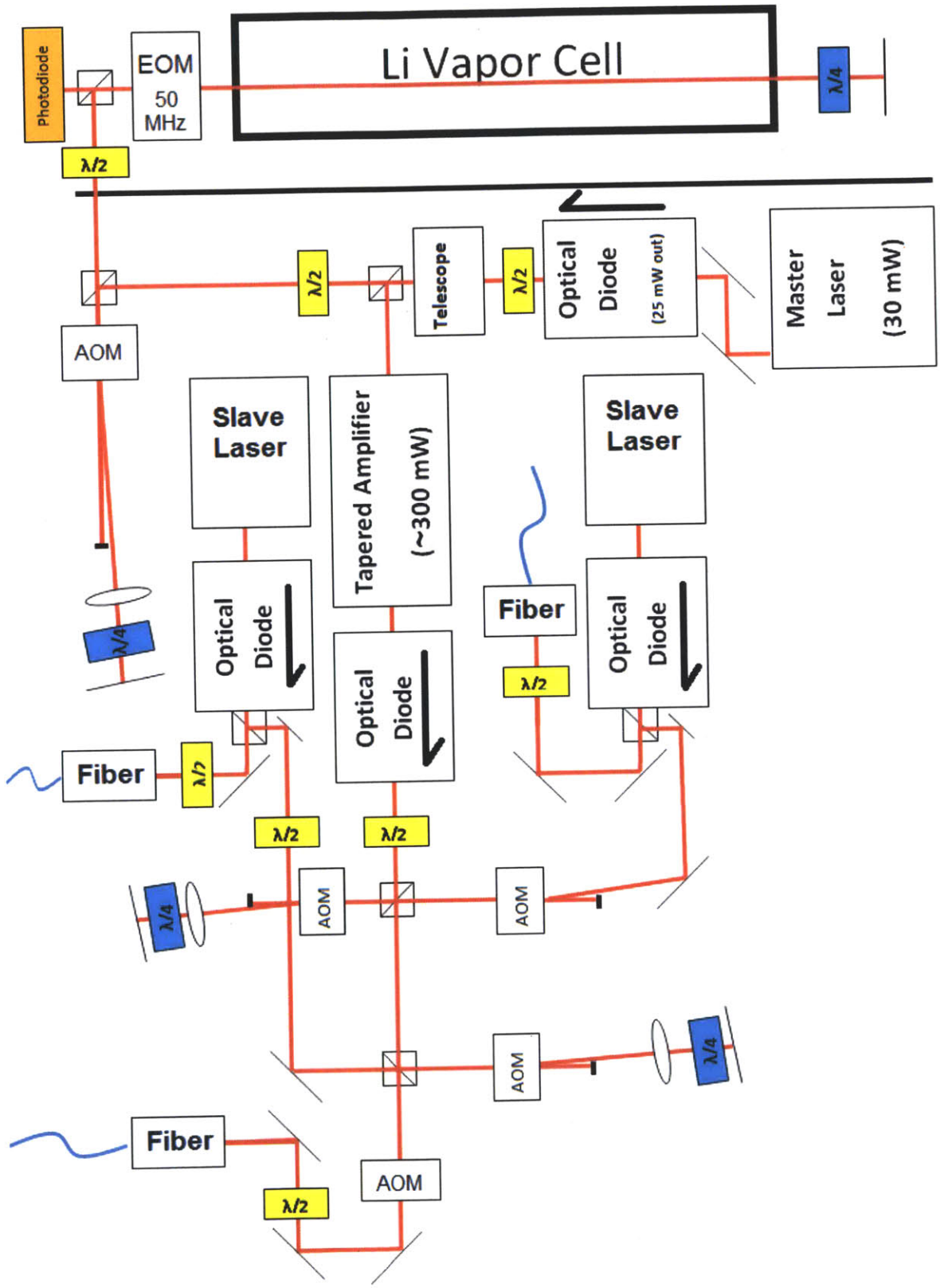

Figure 3-12: Layout of the completed lithium-6 laser system.

Chapter 4

Potassium-40 2D Magneto-Optical Trap

Having described, in the previous chapter, part of the experimental apparatus for cooling and trapping lithium atoms, we now turn to the potassium side of the experiment. In this chapter, we report the achievement of a 2D magneto-optical trap for potassium-40 atoms. The laser system which provides the light which the 2D MOT uses was set up by a visiting graduate student, Thomas Gersdorf, and is documented in his Diploma thesis [29]. At the time of writing, the 2D MOT has been set up and the first atoms have been successfully cooled and trapped. However, the various parameters which affect the performance of the MOT have not yet been optimized. Thus, in this chapter we describe only the setup of the MOT and the initial confirmation that the trapping was achieved.

4.1 MOT Setup

The setup of our 2D MOT is shown in figure 4-1. As described in chapter 2, we use a $2D^+$-MOT, which consists of a MOT in two directions and an optical molasses in the third.

The 2D MOT system described in this chapter is the first one set up in all of the MIT atomic physics laboratories. Previous experiments in our group with fermionic

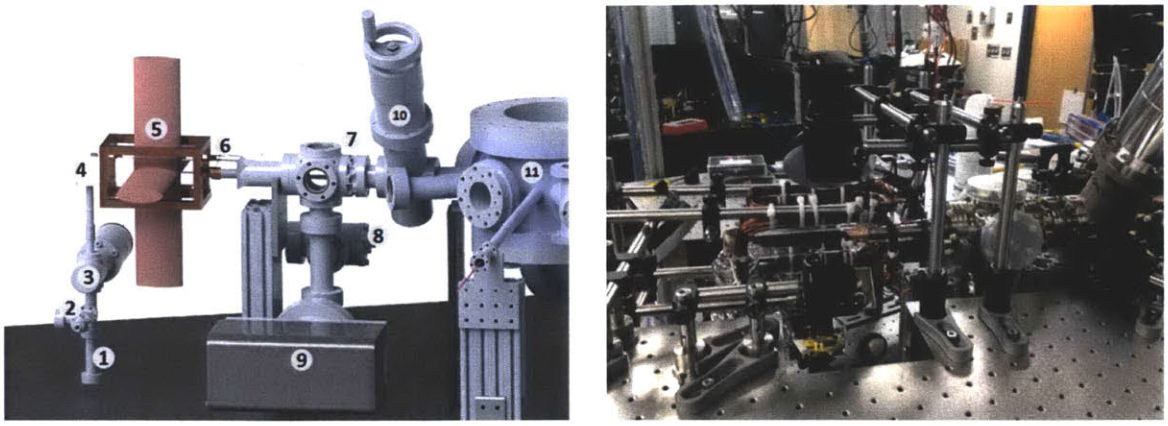

Figure 4-1: (a) a schematic view of the 2D MOT Setup, omitting the push/retarding beams for clarity. Created by Thomas Gersdorf. (b) Our implementation of the 2D MOT. Please pardon the mess.

potassium used a Zeeman slower (see, for example, [30]. It is worth discussing the differences between the two technologies.

The main advantage of a 2D MOT over a Zeeman slower is a higher efficiency, in terms of the atomic flux per original atom number. Zeeman slowers can produce higher fluxes overall, but when efficiency is a concern, the 2D MOT is a better choice. In the case of potassium-40, efficiency is a huge concern: the (very expensive) enriched sample of potassium we use contains only 5% potassium-40. In addition, 2D MOTs produce a smaller stray magnetic field in the main chambers than Zeeman slowers and take up much less space.

4.1.1 Vacuum Chamber

Briefly, the setup depicted in figure 4-1 consists of the following: ① A 50 mg sample of enriched potassium (with 5% ^{40}K abundance) is heated in an ampoule to about 100° C, and diffuses into ④ a glass cell where it is trapped by the magnetic fields and ⑤ circularly-polarized laser beams. Between the potassium ampoule and glass cell are ② a connection for a vacuum pump and ③ an all-metal gate valve for closing off the vacuum chamber to change the potassium sample. After the potassium cloud is trapped in the glass cell, pushing and retarding beams (not shown) shoot the atoms through a hole in the ⑥ copper mirror. In the ⑦ intermediate chamber, the atomic

beam can be analyzed, after which it passes through another ⑩ gate valve into ⑪ the main chamber, where it will be captured in a 3D MOT.

We use heating tapes to achieve the desired temperature of 100° C in the potassium ampoule. Further, we also heat the gate valve and tee, albeit not to such high temperatures. Were we to leave these parts unheated, the hot potassium atoms diffusing out of the ampoule would stick to the cold metal in the gate valve and tee. Typically, we heat both parts to 80° C. Originally, we had planned to heat the glass cell as well, but we found that the thermal conductivity of the chamber was high enough that the cell automatically heated up to about 60° C when the valve and tee were at 80° C.

Because of the heating, the pressure in the glass cell is typically on the order of 10^{-8} - 10^{-7} mbar. In the main chamber, however we require pressures as low as 10^{-11} mbar for sufficient trap lifetimes. To achieve the pressure difference between the main chamber and 2D-MOT chamber, we use so-called differential pumping tubes. These are nothing more than long, thin tubes separating different parts of the chamber. Because the tubes allow very few atoms to pass through them (i.e., they have a low conductivity), they can support large pressure differences across their length. Our 2D MOT setup uses two differential pumping tubes to separate it from the main chamber: first, the hole in the copper mirror supports a pressure ratio of about 10, whereas the tube separating the intermediate chamber from the main chamber supports a pressure ratio of about 100. These differential pumping tubes provide the buffer we need to simultaneously maintain the desired pressures in both the 2D MOT chamber and the main chamber.

4.1.2 Coils

Surrounding the glass cell are the coils which generate the magnetic fields necessary for trapping the atoms. To achieve the desired cigar-shaped trap, the coils are rectangular rather than circular, as they would be in a 3D MOT. Looking back to chapter 2 of this thesis, we know that a single pair of anti-Helmholtz coils is required to generate the magnetic field gradient for the MOT. This pair of coils runs vertically on either

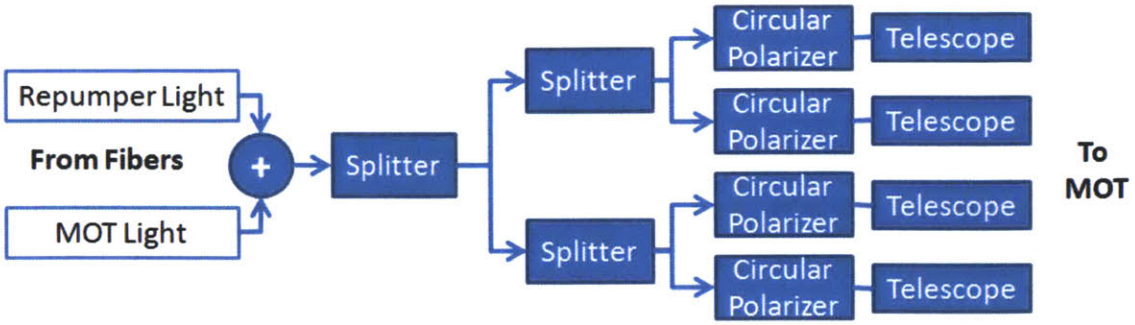

Figure 4-2: Schematic of the 2D MOT optics.

side of the glass cell.

The 2D MOT coils are anchored to posts via cable ties. This is in contrast to coils used in later stages of the experiment (e.g., the 3D MOT coils), which are encased in epoxy and can thus be mounted in a fixed position relative to the vacuum chamber. This sort of mounting scheme is obviously unfeasible for the glass cell. However, because the 2D MOT coils are not so precisely positioned, the magnetic field zero they create may not be in the exact center of the cell. This creates a problem, as we want the 2D MOT cloud to align well with the aperture in the copper mirror.

To circumvent this problem, we use two pairs of so-called offset coils, running both hoizontally and vertically along the length of the glass cell. An offset coil pair consists of two Helmholtz-configured coils and produces a magnetic field which does not change direction (i.e. no zero-crossing) within the glass cell. By adjusting the current running through each pair of offset coils, the magnetic field zero can be moved around within the cell. Thus, by selecting the right values for the offset currents, the MOT can be aligned with the differential pumping tube aperture.

In terms of construction, all of the coils are made using AWG 11 copper wire. The coils are rectangular in shape, 6" by 2.5" in size. Each pair of coils is wired in series and connected to its own power supply; thus, the current in each of the three pairs of coils can be controlled independently.

4.1.3 Optics

The schematic of the optical setup for the 2D MOT is shown in figure 4-2. Fibers from the potassium-40 laser system separately carry MOT light and repumper light to the experiment table. The two beams are combined by overlapping them on a polarization cube, creating one beam with both MOT and repumper frequency components. In this beam both components are linearly polarized, separated by 90°. The combined beam is then split into two by a half-waveplate/polarization-cube combination. The two resulting beams are subsequently split again in the same manner. Four beams result, each with both MOT and repumper light. By adjusting the waveplates, the intensities of the four beams can be tuned relative to each other. Each beam is circularly polarized by passing through a quarter waveplate (two are polarized with a σ_+ helicity and the other two with σ_-), and then shaped by a telescope into an elliptical beam with axes of roughly 2 inches by 1 inch. The beams are then guided by mirrors to overlap on the center of the glass cell.

Pictures of the 2D MOT optics are shown in figures 4-3, 4-4, and 4-5.

4.2 MOT Observation

To observe the trapped cloud of atoms, we placed an infrared CCD camera on the accessible end of the glass cell (opposite the copper mirror), allowing us to measure the fluorescence due to the atoms in the chamber.

When the potassium ampoule, gate valve, and tee were heated to the temperatures previously given, and the optics were switched on, we observed a very bright fluorescence in the chamber, indicating the presence of atoms. To search for a MOT, we switched on the gradient coils (with about 12 A flowing through them) and every two seconds changed the direction of current flow with an H-bridge. This direction flipping was performed for two reasons. First, the polarization of the MOT beams and the direction of the field gradient must match in order for trapping to occur. Rather than keeping track of the directions and thus turning the gradient coils on in the right direction immediately, it is much easier to simply switch directions continuously and

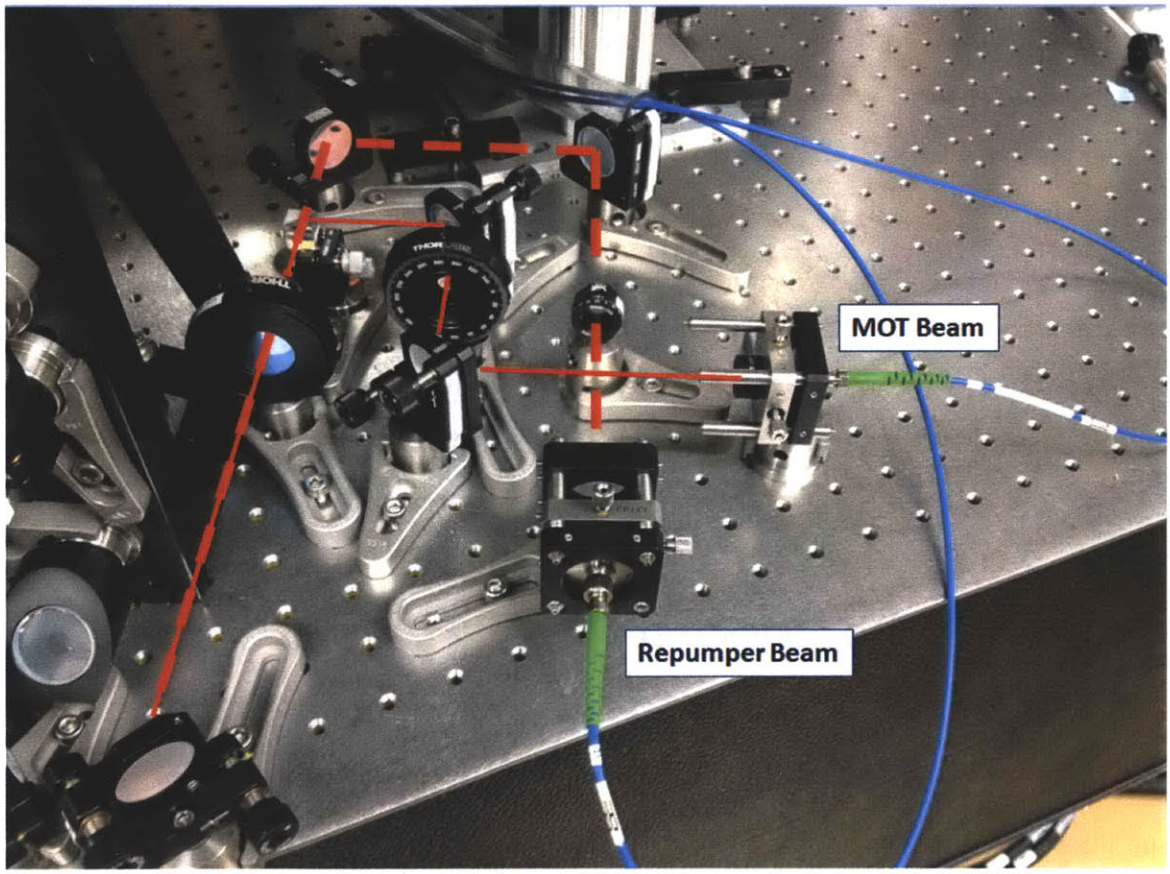

Figure 4-3: Setup for combining the MOT and Repumper beams which come out of fibers from the optical table.

Figure 4-4: After the beams are combined, they are split, circularly polarized, and telescoped on this vertical breadboard.

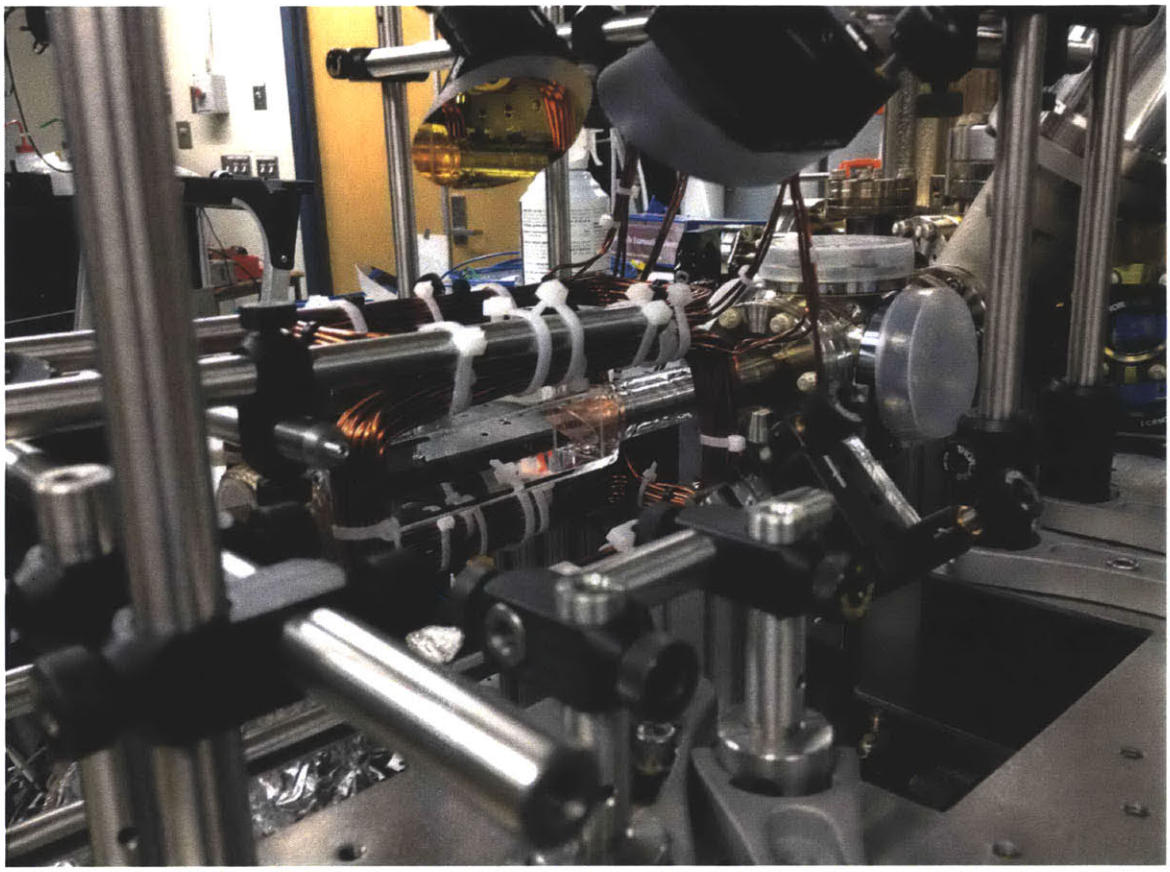

Figure 4-5: The MOT setup, showing the some of the mirrors which align th ebeam in the middle of the glass cell. Also visible is the copper mirror between the glass cell and intermediate chamber.

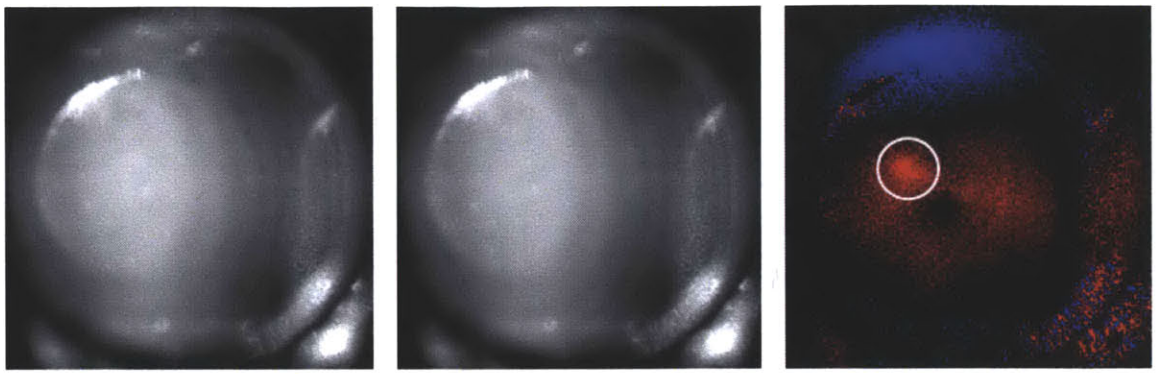

Figure 4-6: (a) 2D MOT fluorescence, (b) fluorescence in the absence of a 2D MOT, and (c) the difference between the two images

search for trapping half of the time. Second, it is easier to discern by eye a changing feature, like a MOT turning off and on, than a static one.

After tuning the laser detunings, beam polarizations/intensities, current magnitude, etc., we finally observed the signature of a 2D MOT, shown in figure 4-6. The figure shows camera images obtained during times when the current through the gradient coil was flowing in opposite directions. The first image, 4-6(a), contains a few-millimeter wide region of high fluorescence, marked by the white circle. The second image, 4-6(b), does not contain such a region. To make this difference more apparent, a subtraction of image (b) from image (a) was performed in MATLAB, resulting in 4-6(c). This image shows a clear difference between the two pictures that indicates the presence of a MOT.

To confirm that we had indeed created a MOT, we performed the following checks. First, we passed current through the horizontal and vertical offset coils, attempting to drag the MOT around the glass cell. We observed that we could, indeed, move the bright spot on the camera around the cell by a few millimeters in each direction. Second, we changed the polarizations of the MOT beams by rotating the quarter waveplate a few degrees (remember, a MOT is sensitive to polarization, whereas a molasses is not). As expected, the spot disappeared when the polarizations were changed, further indicating a MOT. Last, we swept the frequency of the laser beams.

The bright spot disappeared when the laser was swept by only a few MHz, which would only occur if a MOT was present. After all of these checks, we were finally satisfied that we had successfully cooled and trapped the first atoms for the new experiment.

Chapter 5

Conclusion

In this thesis I have outlined my contributions to our group's current experiment, building a quantum gas microscope for fermionic atoms. During the course of this thesis work, a laser system for Zeeman slowing and magneto-optical trapping ^{6}Li atoms was built, although the system has not yet been used to actually cool or trap any atoms. Building such a system, for cooling and trapping alkali atoms, is a standard technique in atomic physics experiment, and a stepping stone towards microscopy. We emphasize that nothing novel was achieved with the construction of this system.

As a further stepping stone towards microscopy, light from an existing laser system for cooling and trapping ^{40}K atoms, built by diploma student Thomas Gersdorf, was used to set up a 2D MOT, as a pre-cooling step towards capturing in a 3D MOT.

Several steps need to be completed before the microscope is ready for action. First, the potassium 2D MOT needs to be optimized to achieve the highest flux of slow atoms into the 3D MOT. This optimization includes not only the adjustment of parameters such as laser beam detunings and magnetic field gradients but also the addition of pushing and retarding beams to the setup.

Once this 2D MOT optimization is complete, optics for the ^{40}K 3D MOT will be set up and optimized. Although the MOT will eventually be a double-species trap, initially all of our experiments will be conducted with potassium. The coils for the MOT have already been built and tested; once the optics are set up, the MOT will

in principle be ready to use.

The MOT is the first stage of our experimental cooling sequence, and it achieves temperatures in the milliKelvin range. This temperature is not sufficient to reach degeneracy, so after the MOT stage, atoms are loaded into a purely magnetic trap. While in this trap, evaporative cooling is performed, resulting in temperatures of about 50 nK, well below the μK scale necessary for degeneracy. After evaporative cooling in the magnetic trap, the atoms will be magnetically transported to the center of our vacuum chamber, where they will be placed in an optical lattice and await microscopy. All of the trapping stages mentioned in this paragraph have yet to be built.

5.1 Outlook

Once the microscope is complete, we will have the capability of exploring novel physics with an unprecedented measurement capability.

5.1.1 Antiferromagnetism

As mentioned previously, one of the avenues we plan to explore is the observation of an antiferromagnet. This observation will lead to further investigations that could ultimately reveal whether or not the Fermi-Hubbard model contains the ingredients of high-temperature superconductivity [15].

5.1.2 Quantum Hall Physics and Topological Insulators

We plan to explore quantum hall physics in an ultracold atomic setting. Using Raman transitions, synthetic magnetic fields can be engineered [31]. This allows us to probe quantum hall physics and topological states of matter. With single-site resolution, we can directly image, for example, edge states characteristic of topological insulators.

5.1.3 Reduced dimensionality

The single optical lattice plane imaged by the quantum gas microscope provides a natural playground for studying strongly interacting fermions in a single 2D plane, which enhances the role of both thermal and quantum fluctuations. One of the new pieces of physics that can be explored in this avenue is the Berezinskii–Kosterlitz–Thouless transition, a phase transition that occurs in two dimensions [32]. Dissociation of vortex pairs is a characteristic of this transition, and our microscope may allow direct in-situ observation of this phenomenon.

Many more avenues of investigation exist, including dipolar molecules in lattices, the formation of exotic lattices such as a honeycomb or Kagome lattice, the simulation of atomtronic circuits, etc. We expect that these explorations will keep us busy for a long time.

Bibliography

[1] M. Gehm, *Preparation of an Optically-Trapped Degenerate Fermi Gas of 6Li: Finding the Route to Degeneracy.* PhD thesis, Duke University, 2003.

[2] T. G. Tiecke, *Feschbach resonances in ultracold mixtures of the fermionic quantum gases 6Li and 40K.* PhD thesis, University of Amsterdam, 2009.

[3] C. Foot, *Atomic Physics.* Oxford University Press, Feb. 2005.

[4] T. Uehlinger, *A 2D Magneto-Optical Trap as a High-Flux Source of Cold Potassium Atoms.* Diploma thesis, Swiss Federal Institute of Technology Zurich, 2008.

[5] A. Ridinger, *Towards quantum degenerate Fermi mixtures: Photoassociation of weakly bound Li-K molecules.* PhD thesis, ENS (Paris), 2011.

[6] S. Campbell, *Building an Apparatus for Ultracold Lithium-Potassium Fermi-Fermi Mixtues.* Undergraduate thesis, Massachusetts Institute of Technology, 2010.

[7] M. W. Zwierlein, *Cooling and Trapping a Bose-Fermi Mixture of Dilute Atomic Gases.* Diploma thesis, Massachusetts Institute of Technology, 2001.

[8] Gary C. Bjorklund, et al., "Frequency modulation (fm) spectroscopy," *Applied Physics B*, vol. 32, no. 145, 1983.

[9] W. Ketterle, D.S. Durfee, and D. M. Stamper-Kurn, "Making, probing, and understanding bose-einstein condenstates," in *Bose-Einstein Condensation in Atomic Gases* (S. S. M. Inguscio and C. Wieman, eds.), Proceedings of the Enrico Fermi Summer School, (Varenna, Italy), July 1998.

[10] R. P. Feynman, "Simulating physics with computers," *International Journal of Theroetical Physics*, vol. 21, no. 6, 1982.

[11] W. Ketterle and M.W. Zwierlein, "Making, probing, and understanding ultracold fermi gases," in *Ultracold Fermi Gases* (W. K. M. Inguscio and C. Salomon, eds.), Proceedings of the Enrico Fermi Summer School, (Varenna, Italy), June 2008.

[12] Waseem S. Bakr, et al., "A quantum gas microscope for detecting single atoms in a hubbard-regime optical lattice," *Nature*, vol. 462, no. 74, 2009.

[13] Jacob F. Sherson, et al., "Single-atom-resolved fluorescence imaging of an atomic mott insulator," *Nature*, vol. 467, no. 68, 2010.

[14] Waseem S. Bakr, et al., "Probing the superfluid to mott insulator transition at the single atom level," *Science*, vol. 329, no. 5991, 2010.

[15] T. Esslinger, "Fermi-hubbard physics with atoms in an optical lattice," *Annu. Rev. Condens. Matter Phy.*, vol. 1, no. 129, 2010.

[16] S. Chu, "The manipulation of neutral particles," *Reviews of Modern Physics*, vol. 70, 1998.

[17] C.N. Cohen-Tannoudji, "Manipulating atoms with photons," *Reviews of Modern Physics*, vol. 70, 1998.

[18] W.D. Phillips, "Laser cooling and trapping of neutral atoms," *Reviews of Modern Physics*, vol. 70, 1998.

[19] C. Cohen-Tannoudji, *Quantum Mechanics: Volumes 1 and 2.* Wiley-Interscience, Oct. 2006.

[20] R. Shankar, *Principles of Quantum Mechanics.* Medford, Massachusetts: Springer, second ed., Sept. 1994.

[21] L. Allen, J.H. Eberly, *Optical Resonance and Two-Level Atoms.* Dover Books on Physics, Dover Publications, 1987.

[22] Harold Metcalf, Peter van der Straten, *Laser Cooling and Trapping.* Sprinter, 1999.

[23] T. W. Hansch, A. L. Schawlow, "Cooling of gases by laser radiation," *Optics Communications*, vol. 13, no. 68, 1975.

[24] O. Svelto, *Principles of Lasers.* Springer, fourth ed., Sept. 2009.

[25] B.E.A. Saleh, M.C. Teich, *Fundamentals of Photonics.* John Wiley and Sons, Aug. 1991.

[26] J. Bechhoefer, "Feedback for physicists: A tutorial essay on control," *Reviews of Modern Physics*, vol. 77, no. 3, 2005.

[27] F. Crawford, *Waves*, vol. 3 of *Berkeley Physics Course.* McGraw-Hill, 1968.

[28] Mini-Circuits, 13 Neptune Ave Brooklyn, NY 11235, *Amplifier: ZHL-1-2W.*

[29] C. T. J. Gersdorf, *A Quantum Gas Microscope for Fermionic Atoms.* Diploma thesis, Massachusetts Institute of Technology, 2012.

[30] Cheng-Hsun Wu, et al., "Strongly interacting isotopic bose-fermi mixture immersed in a fermi sea," *Physical Review A*, vol. 84, no. 1, 2011.

[31] Y.J. Lin, et al., "Synthetic magnetic fields for ultracold neutral atoms," *Nature*, vol. 462, 2009.

[32] J.M. Kosterlitz, D. J. Thouless, "Ordering, metastability and phase transitions in two-dimensional systems," *Journal of Physics C: Solid Stae Physics*, vol. 6, 1973.